Direct uptake mechanism in lysosome required for neuromuscular homeostasis

Yuuki Fujiwara[1,9], Viorica Raluca Contu[1,9], Chihana Kabuta[1,9], Megumu Ogawa[2], Hiromi Fujita[1], Hisae Kikuchi[1], Ryohei Sakai[1], Katsunori Hase[1], Mari Suzuki[3], Ikuko Koyama-Honda[4], Michio Inoue[2,5], Yasushi Oya[6], Yukiko U. Inoue[7], Takayoshi Inoue[7], Ryosuke Takahashi[8], Ichizo Nishino[2,5], Keiji Wada[1], Satoru Noguchi[2,5]*, Tomohiro Kabuta[1]*

[1]Department of Degenerative Neurological Diseases, National Institute of Neuroscience, National Center of Neurology and Psychiatry, Tokyo, Japan, [2]Department of Neuromuscular Research, National Institute of Neuroscience, National Center of Neurology and Psychiatry, Tokyo, Japan, [3]Department of Sensory and Motor Systems, Tokyo Metropolitan Institute of Medical Science, Tokyo, Japan, [4]Department of Biochemistry and Molecular Biology, Graduate School and Faculty of Medicine, The University of Tokyo, Tokyo, Japan, [5]Medical Genome Center, National Center of Neurology and Psychiatry, Tokyo, Japan, [6]Department of Neurology, National Center Hospital, National Center of Neurology and Psychiatry, Tokyo, Japan, [7]Department of Biochemistry and Cellular Biology, National Institute of Neuroscience, National Center of Neurology and Psychiatry, Tokyo, Japan, [8]Department of Neurology, Graduate School of Medicine, Kyoto University, Kyoto, Japan, [9]These authors contributed equally to this work.

*Corresponding authors: e-mail: noguchi@ncnp.go.jp; kabuta@ncnp.go.jp

Regulated degradation of cellular components plays an essential role in homeostasis. Accumulating evidence indicates the importance of lysosomal degradation of cellular proteins[1]: Dysfunctions in multiple pathways to deliver cytosolic substrates into lysosomes are related to various diseases, including cancers, neurodegenerative diseases, and myopathies[2]. However, much of the effort at understanding such pathways has been devoted to studies on macroautophagy, which entails vast and dynamic rearrangement of membrane structure, and knowledge on other delivery systems and functions of lysosomes *per se* remains scant. Here, we show that cytosolic proteins are directly imported into lysosomes by a mechanism distinct from any known pathways and degraded. We find that a lysosomal membrane protein, SIDT2, which was previously reported as a putative nucleic acid transporter, is involved in the translocation of substrate proteins in this system. Gain- and loss-of-function analyses reveal that SIDT2 contributes conspicuously to the lysosomal degradation of a wide range of cytosolic proteins in cells at the constitutive level. Furthermore, a dominant-negative type of mutation in *SIDT2* causes familial rimmed vacuolar myopathy in humans. *Sidt2* knockout mice recapitulated typical features of rimmed vacuolar myopathy, including atrophy and accumulation of cytoplasmic inclusions in skeletal muscles. These results reveal a previously unknown pathway of proteolysis in lysosomes and highlight the importance of noncanonical types of autophagy in human physiology and pathophysiology.

SIDT2 mediates lysosomal proteolysis

Autophagy is a generic term for pathways in which cytosolic components are delivered into lysosomes and degraded[1]. Although low levels of macroautophagy occur at steady-state levels, macroautophagy is primarily a highly inducible phenomenon that responds to stresses such as starvation.[1] Consistent with this, knockdown of *Atg5*, a gene required for macroautophagy, did not have a significant effect on the constitutive level of protein degradation under nutrient-rich conditions in mouse embryonic fibroblasts (MEFs) (Extended Data Fig. 1a). However, the total proteolysis level was markedly decreased in *Atg5*$^{-/-}$ MEFs by specific inhibitors of lysosomal acid proteases, pepstatin A and E64d (Pep+E64) (Extended Data Fig. 1b), suggesting that autophagic pathways other than macroautophagy play an important role in

constitutive protein degradation.

In search of such pathways, we next analysed the degradation levels of proteins in *Atg5*$^{-/-}$ MEFs with the knockdown of genes functioning in other types of autophagy. Knockdown of *Vps4* and *Lamp2a*, genes necessary for microautophagy in late endosome[3,4] and chaperone-mediated autophagy (CMA)[5], respectively, did not have a significant effect on proteolytic activity (Extended Data Fig. 1c). In contrast, knockdown of *Sidt2*, a gene encoding a key factor for the direct uptake and degradation of nucleic acids by lysosomes, RN/DNautophagy (RDA)[6-11], showed a significant decrease of proteolysis in both *Atg5*$^{-/-}$ and *Atg5*$^{+/+}$ MEFs (Fig. 1a, Extended Data Fig. 1c, d, e). SIDT2 is a multi-pass membrane protein that belongs to the putative nucleic acid transporter, systemic RNA interference defective-1 (SID-1) family[12,13]. While we have reported the lysosomal uptake and degradation of nucleic acids via SIDT2[6-11], its function in proteolysis was unknown. The knockdown of *Sidt2* did not affect the level of proteolysis in cells under Pep+E64 treatment, indicating that SIDT2-dependent proteolysis takes place in lysosomes (Fig. 1a, Extended Data Fig. 1d, e). In *Atg5*$^{+/+}$ MEFs, the protein degradation levels under *Sidt2* knockdown were almost equivalent to those in Pep+E64-treated cells (Fig. 1a), indicating that the SIDT2-dependent proteolysis can account for a large proportion of lysosomal degradation of intracellular proteins under nutrient-rich conditions.

In parallel with this, the overall degradation of intracellular protein was markedly accelerated by the overexpression of SIDT2 (Fig. 1b). The degradation levels of individual proteins were further examined using the Tet-Off system in neuro2a (N2A) cells and HeLa cells. The overexpression of SIDT2 markedly accelerated the intracellular degradation of various cytosolic proteins including aggregate-prone proteins, the accumulation of which is implicated in human diseases (Fig. 1c, d, Extended Data Fig. 2a–g). We selected α-synuclein or tau proteins as experimental representative substrates for further examination (Supplementary Text 1). The proteolysis induced by SIDT2 was completely abrogated by Pep+E64 (Fig. 1e). Further, the SIDT2-dependent transport of protein into lysosomes was observed using α-synuclein tagged with fluorescent proteins[14] (Fig. 1f, Extended Data Fig. 3a, b).

A mutant SIDT2 that lacks a lysosomal targeting signals[15] did not accelerate protein degradation (Fig. 1g), indicating that the localization of SIDT2 to the lysosomal membrane is required for the proteolysis via

SIDT2. In RDA, SIDT2 directly binds to substrate nucleic acids via arginine residues in its cytoplasmic loop, and this interaction is necessary for the direct uptake of nucleic acids into lysosomes by SIDT2[16]. Arginine residue is also known to facilitate a wide range of protein–protein interactions through its guanidinium group[17]. We observed that the cytoplasmic domain of SIDT2 also directly binds to α-synuclein protein, and substitution of the arginine residues abolishes both the binding and the degradation of α-synuclein protein (Fig. 1h, i). Furthermore, mutation in the putative hydrolase-active site of SIDT2[18], necessary for its nucleic acid transport[8,9,19], also abolished the SIDT2-dependent proteolysis (Fig. 1j), all of which suggests that protein is imported into lysosomes by SIDT2 via a mechanism similar to that for nucleic acids.

We confirmed that the constitutive activity of macroautophagy is not accelerated upon SIDT2 overexpression (Extended Data Fig. 4a) and that the accelerated proteolysis by SIDT2 is independent of Atg5, as well as Atg13, a macroautophagy-initiation factor (Extended Data Fig. 4b–g). In addition, SIDT2 did not significantly accelerate the degradation of LC3 protein (Extended Data Fig. 4h).

Lysosomal uptake of proteins via SIDT2

The macroautophagy-independent and SIDT2-dependent lysosomal proteolysis led us to a hypothesis that lysosomes may directly take up substrate proteins via SIDT2. To determine this, we performed an *in vitro* reconstruction assay using isolated lysosomes[6-9]. As expected, recombinant α-synuclein and tau protein were directly degraded by isolated lysosomes only in the presence of ATP (Fig. 1k, l, Extended Data Fig. 5a). Importantly, the protein degradation level was attenuated in lysosomes derived from *Sidt2*$^{-/-}$ MEFs (Fig. 1m), and we have confirmed that the lysosomal pH and the proteolytic activity of luminal hydrolases were unaltered (Extended Data Fig. 6a, b). In parallel with this, degradation of the protein was accelerated in lysosomes derived from SIDT2-overexpressing cells (Fig. 1n). The protein degradation was abrogated by the preincubation of lysosomes with Pep+E64, ensuring that the proteolysis occurred in lysosomes (Fig. 1o). We confirmed that lysosomes were retained intact during the incubation (Extended Data Fig. 5b). Under immunoelectron microscopic observation, we found α-synuclein protein directly taken up into the

lysosomal lumen (Fig. 1p, Extended Data Fig. 6c–e). A proportion of substrate protein was partially co-localized with lysosomes even in the absence of ATP, but the degradation of protein was observed only in the presence of ATP (Fig. 1q, Extended Data Fig. 5c). Considering that lysosomal hydrolases do not require ATP[20], this suggests that the step requiring ATP in this system is the import of substrate protein into lysosomal lumen. Taken together, these findings indicate that protein is directly taken up into lysosomes in an ATP-dependent manner via SIDT2 and degraded.

Identification of a novel autophagic pathway

While microautophagy in mammalian cells takes place in late endosomes and little, if any, is observed in lysosomes[3], the direct uptake of protein by CMA has been reported to occur in a specific group of lysosomes[21]. CMA is a selective form of autophagy for the degradation of cytoplasmic proteins harbouring a KFERQ-like motif, which is recognized by hsc70 chaperone, and the proteins are directly imported into lysosomes via a lysosomal membrane protein, LAMP2A[22]. α-Synuclein and GAPDH contain KFERQ-like motifs and are known to be substrates for CMA through these sequences. Using the Tet-Off system, we observed that ΔDQ mutant α-synuclein[23] and ΔNR mutant GAPDH proteins that lack KFERQ-like motifs are nonetheless degraded in an SIDT2-dependent manner at the cellular level (Fig. 2a, b). We also observed that recombinant ΔDQ α-synuclein is also directly degraded by isolated lysosomes in an ATP-dependent manner (Fig. 2c, Extended Data Fig. 5d). Furthermore, unlike CMA, the addition of hsc70 did not show an additive effect on the degradation of α-synuclein protein by isolated lysosomes (Fig. 2d, Extended Data Fig. 5e). Lastly, the knockdown of *Lamp2a* did not have any effect on the SIDT2-dependent degradation of α-synuclein protein in cells (Fig. 2e). Taken together, these findings indicate that SIDT2 mediates the direct uptake and degradation of protein by lysosomes irrespective of CMA (Supplementary Text 2, Extended Data Fig. 7a, b).

Similar to the case for CMA, microautophagy in late endosomes is also partly dependent on the KFERQ-like motif and hsc70 in mammalian cells[3], and also requires Atg13 at least in *Drosophila*[24], suggesting that the SIDT2-dependent proteolysis is neither CMA nor microautophagy. Notably, the SIDT2-dependent

proteolysis also occurred irrespective of *Vps4* knockdown (Fig. 2f), indicating that the pathway is independent of VPS4 and does not belong to microautophagy reported to date in mammalian cells. In addition, the level of SIDT2 in isolated lysosomes remained stable during the direct degradation of protein *in vitro* (Fig. 2g), showing that the invagination of SIDT2 itself into the lysosomal lumen does not occur during the process, and suggesting that SIDT2 does not function in the microautophagic pathway involving an as-yet-unknown mechanism either (Supplementary Text 3).

Taking these findings together, we identified here a novel autophagic pathway that directly delivers proteins into lysosomes, independent of any known forms of autophagy identified to date. Together with our previous findings that lysosomes directly import nucleic acids via a similar mechanism[6-11], we hereafter term such systems by which "lysosome directly delivers diverse cytosolic macromolecules into its lumen via membrane proteins" "direct-uptake-via/through-membrane-protein" (DUMP).

Mutation in SIDT2 is associated with rimmed vacuolar myopathy

Because defects in intracellular degradation systems fundamental to homeostasis often lead to diseases featuring the accumulation of intracellular deposits, typically in neurons and muscles, we speculated that the loss of function of DUMP may be associated with such diseases in humans. We searched our in-house database of whole-exome sequencing data on neuromyopathic patients and found a heterozygous single-base deletion in *SIDT2* in one patient with a familial distal myopathy (Fig. 3a). This patient was a 64-year-old Japanese man with apparent dominant inheritance. Clinically, he was diagnosed with distal myopathy and neuropathy with rimmed vacuoles (Supplementary Text 4). Rimmed vacuolar myopathy (RVM)[25,26] is a myopathy pathologically characterized by the presence of "rimmed vacuoles," cytosolic depositions surrounded by autophagic vacuoles, which occasionally contain a variety of aggregate-prone proteins such as phosphorylated tau, ß-amyloid, ubiquitin and α-synuclein in myofibres[27]. Histopathological analyses also revealed typical features of RVM in his biopsy (Supplementary Text 5, Fig. 3b–f).

Whole-exome sequencing of his genomic DNA revealed the presence of a heterozygous variant, c.2226delG in *SIDT2*. This is predicted to cause frameshift at 743Arg resulting in the loss of 90 amino acid residues

containing two putative transmembrane regions at the C-terminus, which are replaced by 72 amino acid residues with an aberrant sequence (Extended Data Fig. 8a, b). No mutations in genes known to be causative of RVMs were found.

To determine whether this variant in *SIDT2* is pathogenic, we next characterized the molecular properties of this mutant SIDT2. First, we found that the mutant (Δ2226G) SIDT2 is incapable of accelerating intracellular proteolysis (Fig. 3g), even though the mutant protein localized normally to lysosomes (Extended Data Fig. 8c). Further delineation revealed that aberrant hypoglycosylation occurred in Δ2226G SIDT2 (Extended Data Fig. 8d). Notably, we found that the glycosylation of wild-type (WT) SIDT2 was also predominantly decreased to the same level upon co-expression with Δ2226G mutant (Fig. 3h, Extended Data Fig. 8d), indicating that the co-expression of Δ2226G SIDT2 led to a similar change in post-translational modification of WT SIDT2. We further confirmed that the level of the upper band of SIDT2 protein was decreased while that of the lower band was increased in a muscle biopsy of the patient, particularly in immunoblotting specific to both WT and the mutant SIDT2 (Fig. 3i, j). We confirmed that the WT and the mutant SIDT2 transcripts are expressed at equivalent levels in the patient (Extended Data Fig. 8a). From these observations, we speculated that Δ2226G SIDT2 may be pathogenic and have a dominant-negative effect. Strikingly, the co-expression of Δ2226G SIDT2 with WT SIDT2 severely impaired the acceleration of proteolysis by WT (Fig. 3k). All of these observations strongly suggested that SIDT2-dependent proteolysis is reduced in the patient's muscle and provided a convincing explanation for the pathological features seen in the patient. Taking these findings together, loss of function of SIDT2 causes RVM in humans.

DUMP deficiency resulted in RVM-like phenotypes

To investigate whether dysfunction of SIDT2 can in fact induce myopathy and to elucidate the impact of DUMP *in vivo*, we next generated SIDT2-deficient mice using the CRISPR/Cas9 system (Extended Data Fig. 9a). Strikingly, the SIDT2-deficient mice recapitulated the typical symptoms of RVM, analogous to those seen in the patient (Supplementary Text 6, Fig. 4a–h, Extended Data Fig. 9b–e). Because diseases

with rimmed vacuoles share commonalities in their pathogenesis with impaired protein catabolism and intracellular deposit formation [26], we speculated that the deficiency of SIDT2 could cause RVM through the impairment of DUMP (Supplementary Text 7). Indeed, we observed that the degradation of proteins by DUMP was almost completely abrogated in lysosomes derived from *Sidt2*$^{-/-}$ muscles (Fig. 4i). The level of RNA degradation by DUMP (RNautophagy) was also attenuated in lysosomes derived from *Sidt2*$^{-/-}$ muscles (Extended Data Fig. 9f). This is consistent with the observation that various RNAs were also accumulated in the *Sidt2*$^{-/-}$ muscles (Extended Data Fig. 9g). These findings indicate that loss of function of SIDT2 results in DUMP deficiency, which causes an RVM-like phenotype *in vivo* (Supplementary Text 8, Extended Data Fig. 9h, i).

Discussion

Taken together, our data show that lysosomes directly import proteins into their lumen in a mechanism distinct from any known forms of autophagy and SIDT2 translocates substrate proteins in this pathway (Extended Data Figure 10). The direct transport of protein through membrane proteins is also known in organelles other than lysosomes, such as mitochondria, endoplasmic reticulum, and peroxisomes, all of which are mediated by multi-pass membrane proteins that form translocon pores capable of transporting proteins even in a folded state[28]. The precise mechanism by which SIDT2, which was initially reported as a nucleic acid transporter, mediates the uptake of proteins remains to be clarified. Preceding studies on the flexibility of translocon pores in other organelles, as well as other transporters, may help to resolve this issue. For example, arginine residues play a pivotal role in the recognition of substrate peptides in proton-dependent oligopeptide transporters (POTs)[29]. POTs are capable of transporting almost all kinds of di/tripeptides and even therapeutic agents, and their high polyspecificity is attributed to arginine, lysine, glutamate and tyrosine residues in their substrate-binding sites[29], all of which are also enriched in the cytosolic domain of SIDT2 (Fig. 1h). Further studies on the crystal structure of SIDT2 and possible cofactors may also be required to delineate this point. High polyspecificity is also known in transporters for smaller molecules, such as aquaporins. Aquaporins transport multiple types of molecules that do not

even share similarities in structure, such as ammonia, silicic acid and even glycerol[30].

The human patient harbouring c.2226delG mutation in SIDT2 and the typical features of RVM seen in the *Sidt2*$^{-/-}$ mice provide further insight into the physiological and pathophysiological role of this pathway *in vivo*. The late onset and slow progression of the disease are features often observed in RVMs, as seen in the patient reported here. Proteostasis in skeletal muscle under DUMP deficiency may be sustained during younger ages through other cellular mechanisms including macroautophagy, unfolded protein response in endoplasmic reticulum and the ubiquitin–proteasome system. The defects of the latter two mechanisms have also been implicated in the pathogenesis of RVMs. DUMP may be one of the integrated systems for proteostasis in postmitotic long-lived tissues, such as muscles and neurons. Such systems are thought to be particularly important for the quality control of cellular proteins in stress conditions including aging and diseases. DUMP may provide a novel target for therapeutic intervention for degenerative diseases in muscles and neurons.

References

1 Mizushima, N. & Komatsu, M. Autophagy: renovation of cells and tissues. *Cell* **147**, 728-741 (2011).

2 Mizushima, N., Levine, B., Cuervo, A. M. & Klionsky, D. J. Autophagy fights disease through cellular self-digestion. *Nature* **451**, 1069-1075 (2008).

3 Sahu, R. *et al.* Microautophagy of cytosolic proteins by late endosomes. *Dev. Cell* **20**, 131-139 (2011).

4 Mejlvang, J. *et al.* Starvation induces rapid degradation of selective autophagy receptors by endosomal microautophagy. *J Cell Biol* **217**, 3640-3655 (2018).

5 Cuervo, A. M. & Dice, J. F. A receptor for the selective uptake and degradation of proteins by lysosomes. *Science* **273**, 501-503 (1996).

6 Fujiwara, Y. *et al.* Discovery of a novel type of autophagy targeting RNA. *Autophagy* **9**, 403-409 (2013).

7 Fujiwara, Y. *et al.* Direct uptake and degradation of DNA by lysosomes. *Autophagy* **9**, 1167-1171 (2013).

8 Aizawa, S. *et al.* Lysosomal putative RNA transporter SIDT2 mediates direct uptake of RNA by lysosomes. *Autophagy* **12**, 565-578 (2016).

9 Aizawa, S. *et al.* Lysosomal membrane protein SIDT2 mediates the direct uptake of DNA by lysosomes. *Autophagy* **13**, 218-222 (2017).

10 Fujiwara, Y., Wada, K. & Kabuta, T. Lysosomal degradation of intracellular nucleic acids—multiple autophagic pathways. *J Biochem* **161**, 145-154 (2017).

11 Yim, W. W. & Mizushima, N. Lysosome biology in autophagy. *Cell Discov* **6**, 6 (2020).

12 Feinberg, E. H. & Hunter, C. P. Transport of dsRNA into cells by the transmembrane protein SID-1. *Science* **301**, 1545-1547 (2003).

13 Jialin, G., Xuefan, G. & Huiwen, Z. SID1 transmembrane family, member 2 (Sidt2): a novel lysosomal membrane protein. *Biochem Biophys Res Commun* **402**, 588-594 (2010).

14 Katayama, H., Yamamoto, A., Mizushima, N., Yoshimori, T. & Miyawaki, A. GFP-like proteins stably accumulate in lysosomes. *Cell Struct Funct* **33**, 1-12 (2008).

15 Contu, V. R. *et al.* Lysosomal targeting of SIDT2 via multiple YxxΦ motifs is required for SIDT2 function in the process of RNautophagy. *J Cell Sci* **130**, 2843-2853 (2017).

16 Hase, K. *et al.* Cytosolic domain of SIDT2 carries an arginine-rich motif that binds to RNA/DNA and is important for the direct transport of nucleic acids into lysosomes. *Autophagy*, 1-15 (2020).

17 Crowley, P. B. & Golovin, A. Cation-pi interactions in protein-protein interfaces. *Proteins* **59**, 231-239 (2005).

18 Pei, J., Millay, D. P., Olson, E. N. & Grishin, N. V. CREST--a large and diverse superfamily of putative transmembrane hydrolases. *Biol Direct* **6**, 37 (2011).

19 Shih, J. D. & Hunter, C. P. SID-1 is a dsRNA-selective dsRNA-gated channel. *RNA* **17**, 1057-1065 (2011).

20 Coffey, J. W. & De Duve, C. Digestive activity of lysosomes. I. The digestion of proteins by extracts of rat liver lysosomes. *J Biol Chem* **243**, 3255-3263 (1968).

21 Cuervo, A. M., Dice, J. F. & Knecht, E. A population of rat liver lysosomes responsible for the

selective uptake and degradation of cytosolic proteins. *J Biol Chem* **272**, 5606-5615 (1997).

22 Kaushik, S. & Cuervo, A. M. The coming of age of chaperone-mediated autophagy. *Nat Rev Mol Cell Biol* **19**, 365-381 (2018).

23 Cuervo, A. M., Stefanis, L., Fredenburg, R., Lansbury, P. T. & Sulzer, D. Impaired degradation of mutant alpha-synuclein by chaperone-mediated autophagy. *Science* **305**, 1292-1295 (2004).

24 Mukherjee, A., Patel, B., Koga, H., Cuervo, A. M. & Jenny, A. Selective endosomal microautophagy is starvation-inducible in Drosophila. *Autophagy* **12**, 1984-1999 (2016).

25 Nishino, I. Autophagic vacuolar myopathies. *Curr Neurol Neurosci Rep* **3**, 64-69 (2003).

26 Nonaka, I., Noguchi, S. & Nishino, I. Distal myopathy with rimmed vacuoles and hereditary inclusion body myopathy. *Curr Neurol Neurosci Rep* **5**, 61-65 (2005).

27 Malicdan, M. C., Noguchi, S., Nonaka, I., Hayashi, Y. K. & Nishino, I. A Gne knockout mouse expressing human GNE D176V mutation develops features similar to distal myopathy with rimmed vacuoles or hereditary inclusion body myopathy. *Hum Mol Genet* **16**, 2669-2682 (2007).

28 Schnell, D. J. & Hebert, D. N. Protein translocons: multifunctional mediators of protein translocation across membranes. *Cell* **112**, 491-505 (2003).

29 Newstead, S. Towards a structural understanding of drug and peptide transport within the proton-dependent oligopeptide transporter (POT) family. *Biochem Soc Trans* **39**, 1353-1358 (2011).

30 Wu, B. & Beitz, E. Aquaporins with selectivity for unconventional permeants. *Cell Mol Life Sci* **64**, 2413-2421 (2007).

31 Kuma, A. *et al.* The role of autophagy during the early neonatal starvation period. *Nature* **432**, 1032-1036 (2004).

32 Kaizuka, T. *et al.* An Autophagic Flux Probe that Releases an Internal Control. *Mol Cell* **64**, 835-849 (2016).

33 Kaizuka, T. & Mizushima, N. Atg13 Is Essential for Autophagy and Cardiac Development in Mice. *Mol Cell Biol* **36**, 585-595 (2016).

34 Hase, K. *et al.* RNautophagy/DNautophagy possesses selectivity for RNA/DNA substrates. *Nucleic*

Acids Res **43**, 6439-6449 (2015).

35 Endo, Y. *et al.* Dominant mutations in ORAI1 cause tubular aggregate myopathy with hypocalcemia via constitutive activation of store-operated Ca(2)(+) channels. *Hum Mol Genet* **24**, 637-648 (2015).

36 Malicdan, M. C., Noguchi, S. & Nishino, I. Monitoring autophagy in muscle diseases. *Methods Enzymol* **453**, 379-396 (2009).

37 Noguchi, S., Ogawa, M., Malicdan, M. C., Nonaka, I. & Nishino, I. Muscle Weakness and Fibrosis Due to Cell Autonomous and Non-cell Autonomous Events in Collagen VI Deficient Congenital Muscular Dystrophy. *EBioMedicine* **15**, 193-202 (2017).

38 Nguyen, H. T. *et al.* Small-Vessel Vasculopathy Due to Aberrant Autophagy in LAMP-2 Deficiency. *Sci Rep* **8**, 3326 (2018).

39 Cho, A. *et al.* Sialic acid deficiency is associated with oxidative stress leading to muscle atrophy and weakness in GNE myopathy. *Hum Mol Genet* **26**, 3081-3093 (2017).

40 Malicdan, M. C., Noguchi, S., Hayashi, Y. K. & Nishino, I. Muscle weakness correlates with muscle atrophy and precedes the development of inclusion body or rimmed vacuoles in the mouse model of DMRV/hIBM. *Physiol Genomics* **35**, 106-115 (2008).

41 Malicdan, M. C., Noguchi, S., Hayashi, Y. K., Nonaka, I. & Nishino, I. Prophylactic treatment with sialic acid metabolites precludes the development of the myopathic phenotype in the DMRV-hIBM mouse model. *Nat Med* **15**, 690-695 (2009).

42 Komatsu, M. *et al.* Impairment of starvation-induced and constitutive autophagy in Atg7-deficient mice. *J Cell Biol* **169**, 425-434 (2005).

43 Azhar, M. *et al.* Myocardial deletion of Smad4 using a novel alpha skeletal muscle actin Cre recombinase transgenic mouse causes misalignment of the cardiac outflow tract. *Int J Biol Sci* **6**, 546-555 (2010).

44 Malicdan, M. C., Noguchi, S. & Nishino, I. Autophagy in a mouse model of distal myopathy with rimmed vacuoles or hereditary inclusion body myopathy. *Autophagy* **3**, 396-398 (2007).

Figures and Figure Legends

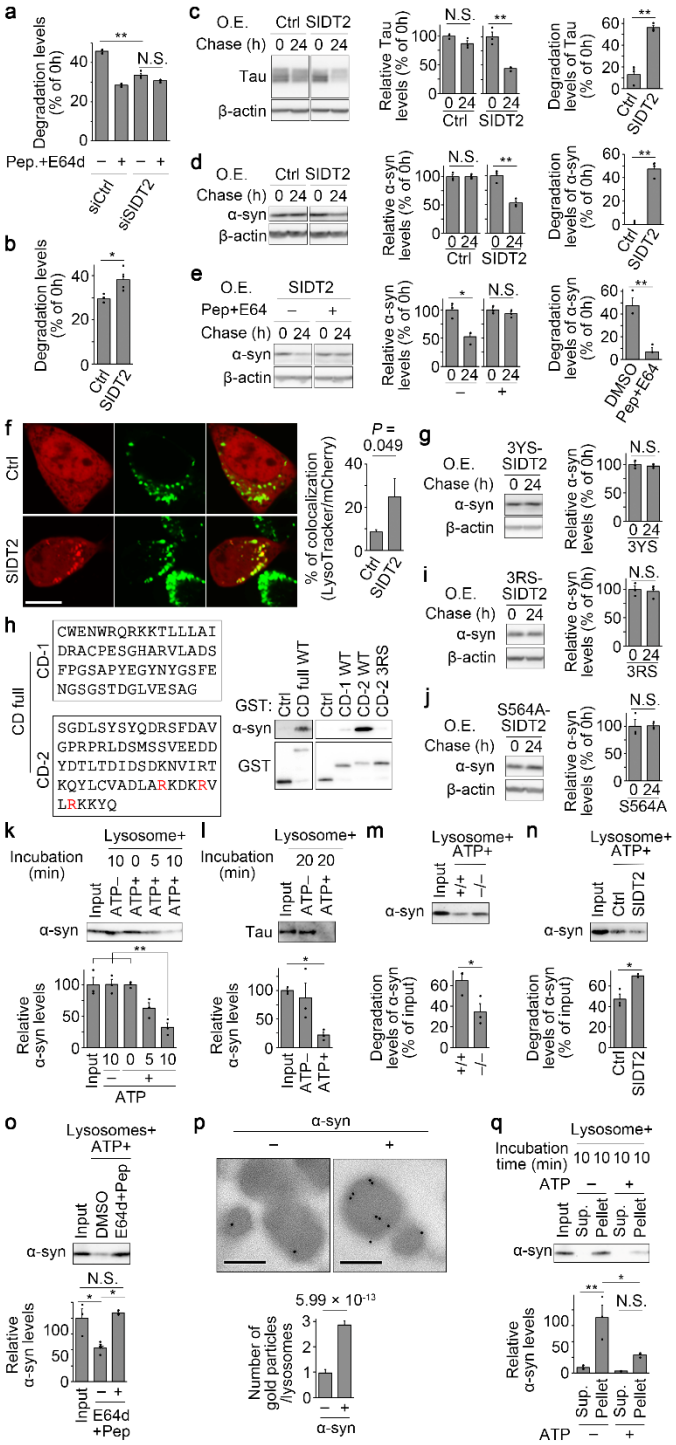

Fig. 1 SIDT2 mediates lysosomal proteolysis through direct uptake of protein into lysosomes.

a, Effect of *Sidt2* knockdown and lysosomal protease inhibitors on the degradation levels of radiolabelled total proteins in *Atg5*$^{+/+}$ MEFs (n = 4). b, Effect of SIDT2 overexpression on the degradation levels of

radiolabelled total proteins in N2A cells (n = 4). c, d, Degradation levels of tau (c) and α-synuclein (d) protein in N2A cells overexpressing SIDT2, using the Tet-Off system (n = 3). O.E.: overexpression. e, Degradation levels of α-synuclein protein in SIDT2-overexpressing N2A cells incubated with or without lysosomal protease inhibitors (n = 3). f, Localization of α-synuclein–mCherry protein in SIDT2-overexpressing N2A cells (control n = 14, SIDT2 n = 12). Bar represents 10 μm. g, Degradation levels of α-synuclein protein in N2A cells overexpressing mutant SIDT2 that lacks lysosome targeting signals (n = 3). h, Interaction of the cytosolic domain of SIDT2 with α-synuclein protein. i, Degradation levels of α-synuclein protein in N2A cells overexpressing mutant SIDT2 that lacks the capacity to bind to α-synuclein protein (n = 3). j, Degradation levels of α-synuclein protein in N2A cells overexpressing mutant SIDT2 that lacks a putative hydrolase-active site (n = 3). k, l, Degradation of α-synuclein (k) and tau (l) protein by isolated lysosomes derived from *Atg5*$^{+/+}$ MEFs (n = 3). m, n, o, Degradation levels of α-synuclein protein by isolated lysosomes derived from SIDT2$^{+/+}$ and SIDT2$^{-/-}$ MEFs (m), from SIDT2-overexpressing N2A cells (n), or from *Atg5*$^{+/+}$ MEFs (o). Isolated lysosomes were preincubated with or without Pep+E64 (o). p, Immunoelectron microscopy image of α-synuclein protein in isolated lysosomes co-incubated with or without recombinant α-synuclein protein in the presence of ATP. Bars represent 200 nm. q, Levels of α-synuclein protein after incubation with isolated lysosomes derived from *Atg5*$^{+/+}$ MEFs in the presence or absence of ATP, followed by separation of lysosomal pellet and external solution (n = 3). *$p < 0.05$, **$p < 0.001$.

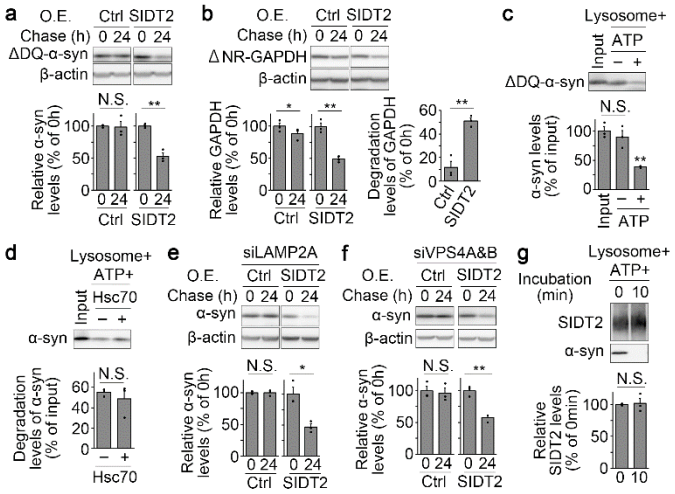

Fig. 2 SIDT2-dependent lysosomal proteolysis is independent of any canonical types of autophagy.

a, b, Degradation levels of mutant α-synuclein (a) and GAPDH (b) protein that lacks the KFERQ-like motif in N2A cells overexpressing SIDT2, using the Tet-Off system (n = 3). c, Degradation of recombinant mutant α-synuclein protein that lacks the KFERQ-like motif by isolated lysosomes (n = 3). d, Degradation levels of recombinant WT α-synuclein protein by isolated lysosomes with or without Hsc70 chaperone (n = 3). e, f, Degradation levels of α-synuclein protein in SIDT2-overexpressing N2A cells treated with siRNA against *Lamp2a* (e) or *Vps4a* and *b* (f) (n = 3). g, Levels of SIDT2 in isolated lysosomes before and after the incubation (n = 3). *p < 0.05, **p < 0.001.

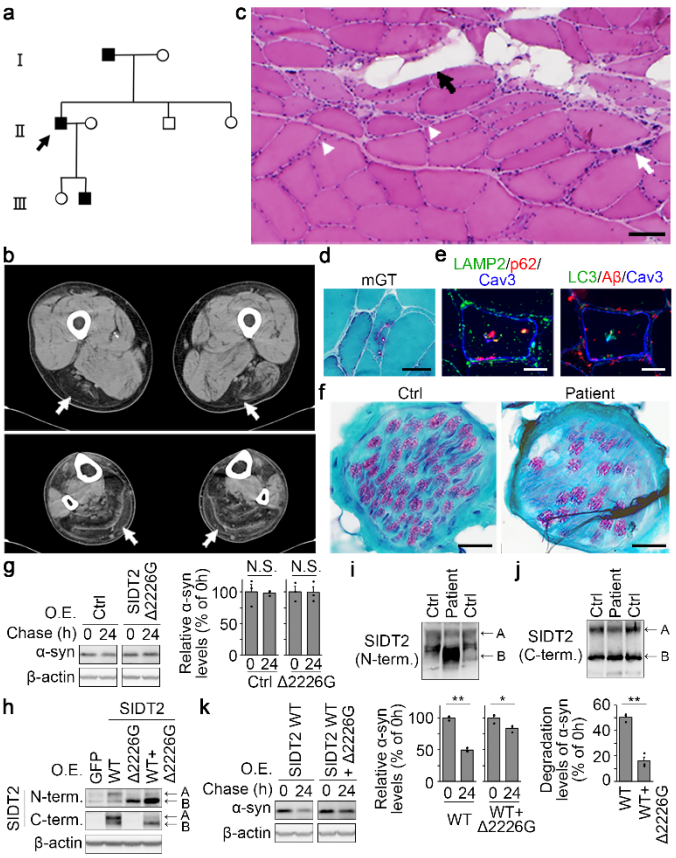

Fig. 3 Loss of function of SIDT2 causes rimmed vacuolar myopathy in humans.

a, Pedigree chart of the proband and family affected by myopathy. The proband is indicated with an arrow. b, Computed tomography (CT) image of the legs of the patient. The white arrow indicates the lesion. c, Haematoxylin and eosin (HE)-stained section of skeletal muscle of the patient. The white arrowheads indicate small angular fibres, the white arrow indicates pyknotic nuclear clump, and the black arrow indicates adipose tissue infiltration. d, Modified Gomori trichrome (mGT)-stained section of skeletal muscle of the patient showing rimmed vacuoles. e, Immunohistochemistry of skeletal muscle of the patient. f, mGT section of peripheral nerve in skeletal muscles of a control and the patient biopsy. g, Degradation levels of α-synuclein protein in cells overexpressing Δ2226G mutant SIDT2, using the Tet-Off system (n = 3). h, Immunoblotting of N2A cell lysate overexpressing WT, Δ2226G mutant, or WT and Δ2226G mutant SIDT2 together, using specific antibodies against either the N-terminus or the C-terminus of SIDT2. i, j, Immunoblotting of skeletal muscle of the patient using specific antibodies to either the N-terminus (i) or the C-terminus (j) of SIDT2. k, Degradation levels of α-synuclein protein in cells coexpressing WT and

Δ2226G mutant SIDT2, compared with WT SIDT2 alone (n = 3). Bars represent 40 μm. *$p < 0.05$, **$p < 0.001$.

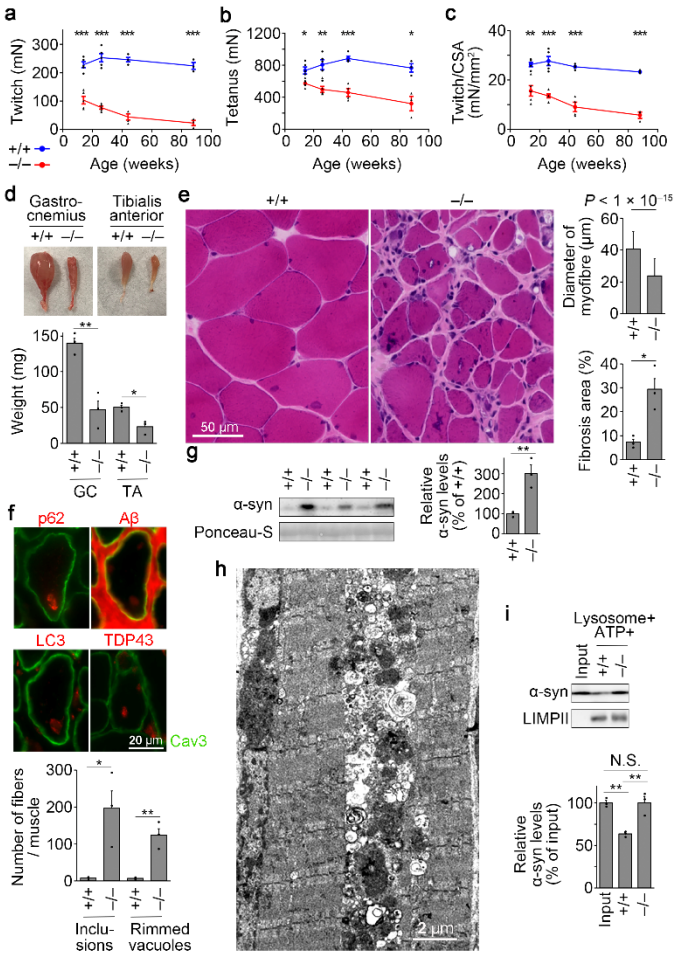

Fig. 4 *Sidt2* deficiency abrogates DUMP activity in skeletal muscle and promotes rimmed-vacuolar myopathic phenotype in mouse.

a–c, Changes in muscle contractions of gastrocnemius in *Sidt2*$^{+/+}$ and *Sidt2*$^{-/-}$ mice. Twitch (a), Tetanus (b) and Twitch/SCA (c) (n = 3–5). d, Skeletal muscles of *Sidt2*$^{+/+}$ and *Sidt2*$^{-/-}$mice and their weight (n = 3). e, HE sections of skeletal muscles of *Sidt2*$^{+/+}$and *Sidt2*$^{-/-}$ mice and their quantification. Diameter of myofibre, +/+: n = 6,258, –/–: n = 5,350 from 3 mice. Fibrosis area, n = 3. f, Immunohistochemistry of skeletal muscles of *Sidt2*$^{+/+}$ and *Sidt2*$^{-/-}$ mice (n = 3). g, Immunoblotting of α-synuclein protein in skeletal muscles of *Sidt2*$^{+/+}$ and *Sidt2*$^{-/-}$ mice (n = 3). h, Electron microscopy image of the ultrastructure of cytoplasmic inclusions in skeletal muscle of *Sidt2*$^{-/-}$ mouse. i, Degradation levels of α-synuclein protein by isolated lysosomes derived from skeletal muscles of WT or *Sidt2*$^{-/-}$ mice (n = 3). *p < 0.05, **p < 0.001, ***p < 0.0001.

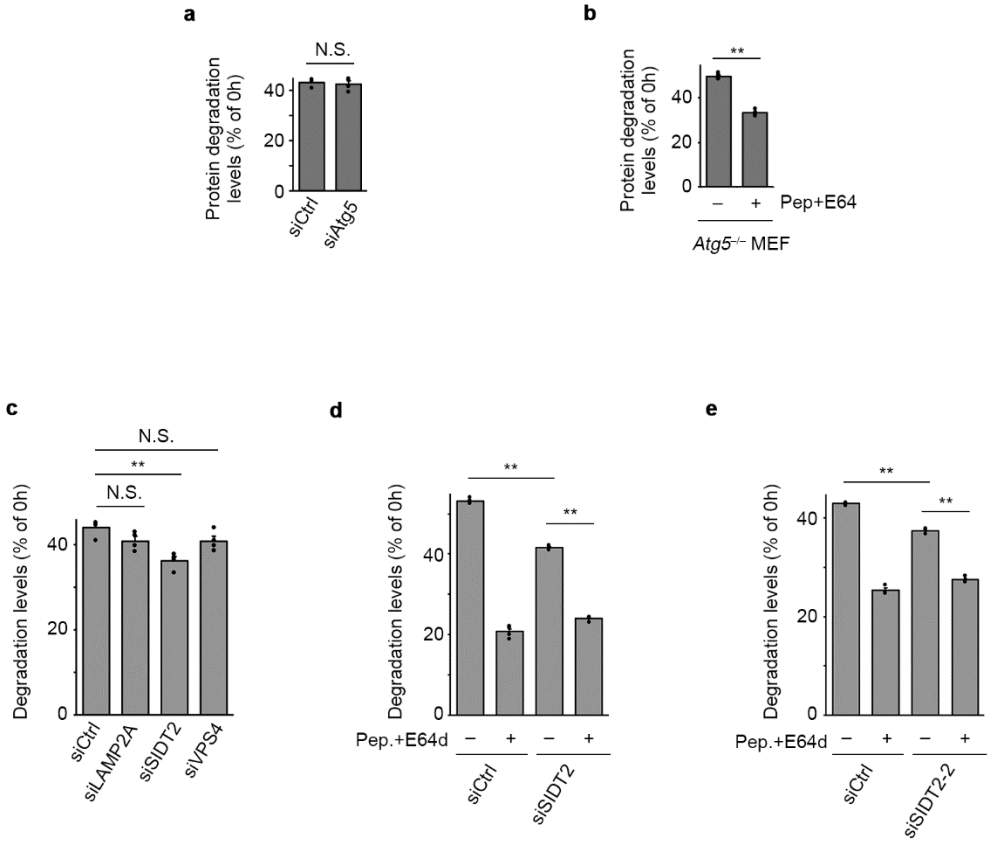

Extended Data Fig. 1 Contribution of SIDT2 and other genes related to canonical types of autophagy at the steady-state level of proteolysis.

a, Effect of *Atg5* knockdown on the degradation levels of radiolabelled total proteins in *Atg5*$^{+/+}$ MEFs (n = 4). b, Effect of lysosomal protease inhibitors on the degradation levels of radiolabelled total proteins in *Atg5*$^{-/-}$ MEFs (n = 4). c, Effect of *Lamp2A*, *Sidt2*, or *Vps4a* and *b* knockdown on degradation levels of radiolabelled total proteins in *Atg5*$^{-/-}$ MEFs (n = 4). d, e, Effect of *Sidt2* knockdown and lysosomal protease inhibitors on degradation levels of radiolabelled total proteins in *Atg5*$^{-/-}$ MEFs, using two different siRNAs against SIDT2 (n = 4). **p < 0.001.

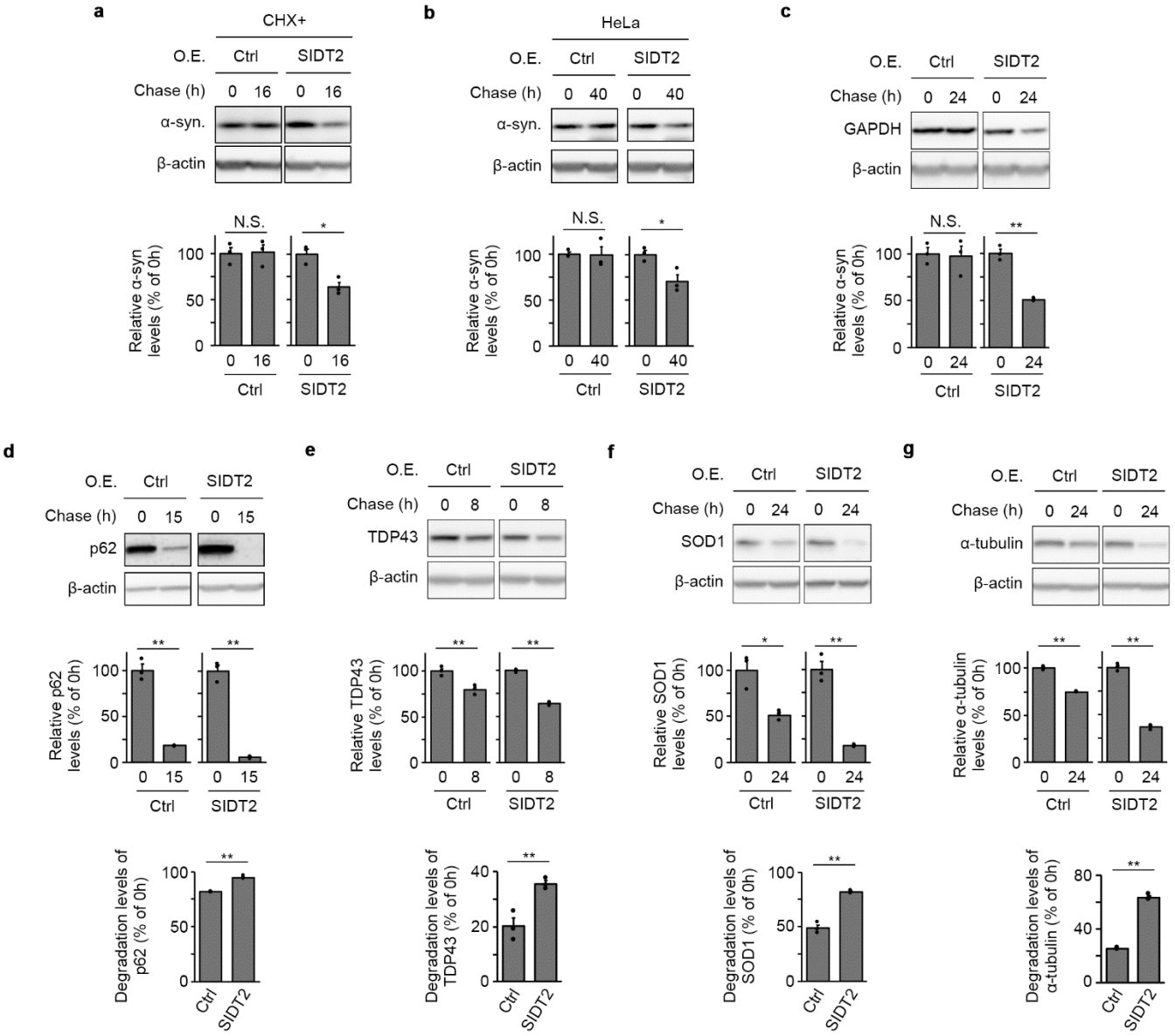

Extended Data Fig. 2 SIDT2 mediates lysosomal degradation of various proteins.

a, Degradation levels of α-synuclein protein in N2A cells overexpressing SIDT2 using the Tet-Off system, under cycloheximide treatment to additionally inhibit protein synthesis during the chase (n = 3). b, Degradation levels of α-synuclein protein in HeLa cells overexpressing SIDT2, using the Tet-Off system (n = 3). c–g, Degradation levels of GAPDH (c), p62 (d), TDP43 (e), SOD1 (f) and α-tubulin (g) proteins in N2A cells overexpressing SIDT2, using the Tet-Off system (n = 3). *$p < 0.05$, **$p < 0.001$.

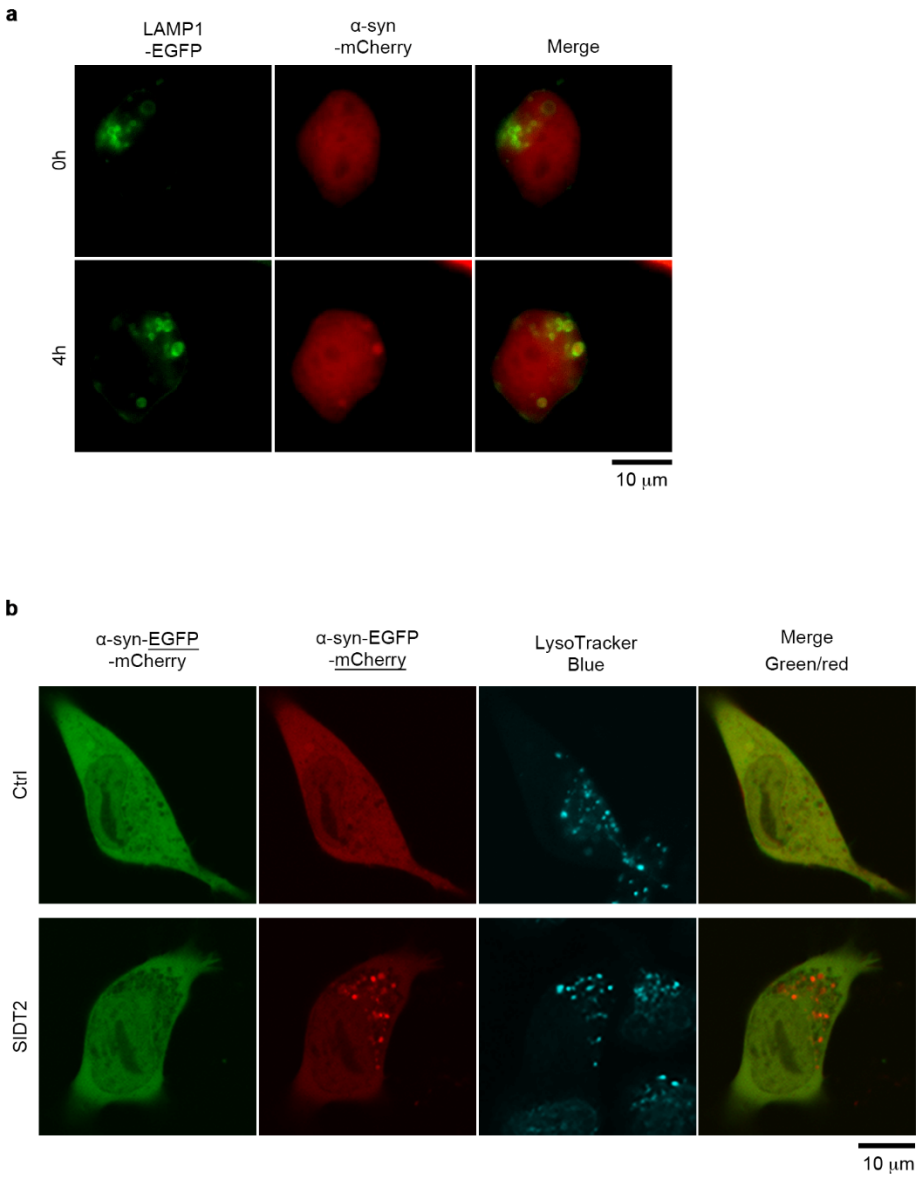

Extended Data Fig. 3 Localization of fluorescent protein-labelled α-synuclein protein in SIDT2-overexpressing cells.

a, Time-lapse imaging of α-synuclein–mCherry in an N2A cell overexpressing SIDT2. α-Synuclein–mCherry is primarily distributed in a diffuse state, and then subsequently translocates to lysosomes. b, Localization of α-synuclein–EGFP–mCherry protein in SIDT2-overexpressing N2A cells. EGFP-negative but mCherry-positive puncta that localize to lysosomes indicate that the protein is imported into the lumen of lysosomes.

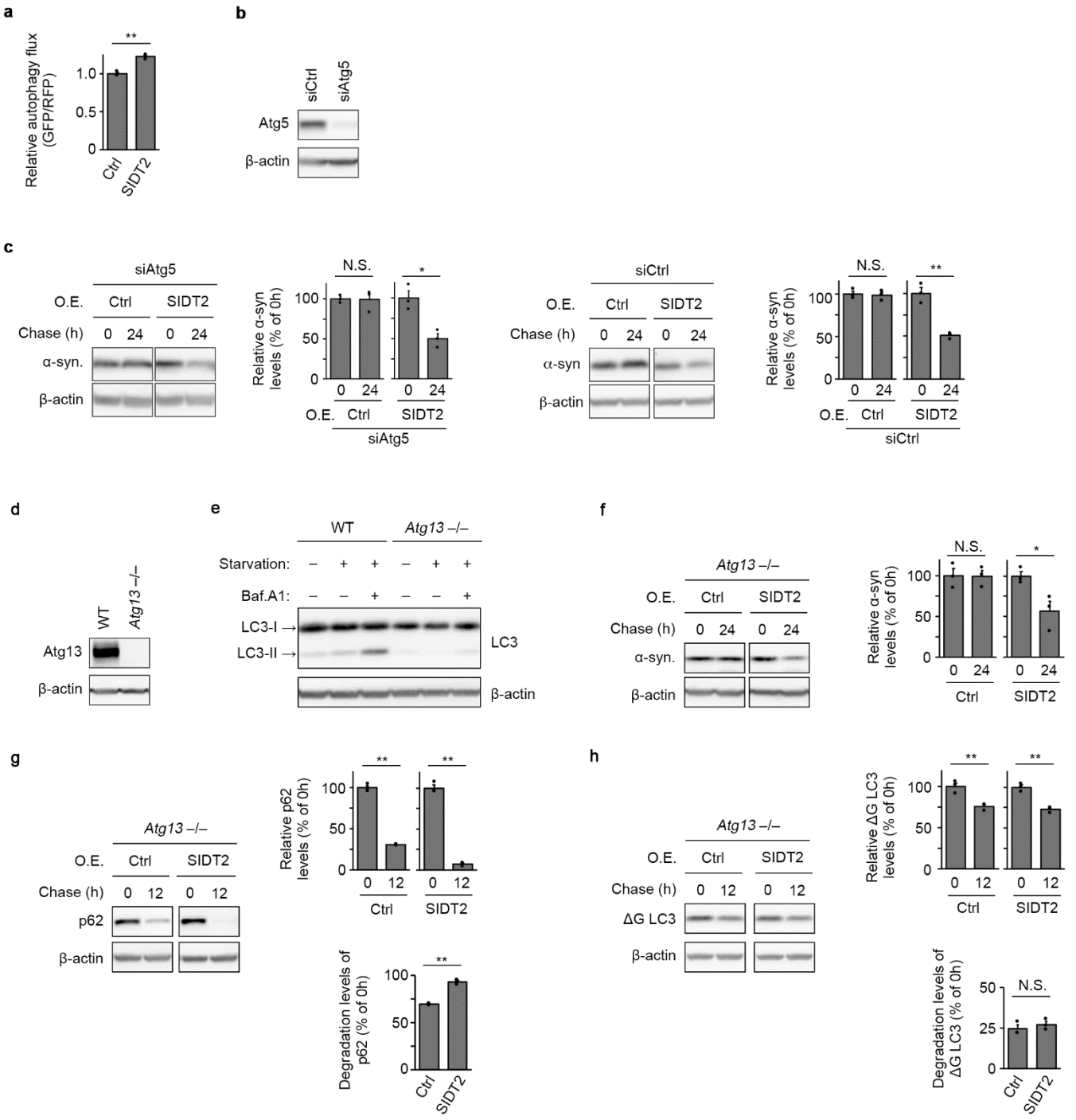

Extended Data Fig. 4 SIDT2-dependent proteolysis is independent of macroautophagy.

a, Autophagic flux in N2A cells overexpressing SIDT2 (n = 3). The higher GFP/RFP ratio indicates lower activity of macroautophagy. b, Immunoblotting of Atg5 in N2A cells treated with siRNA against *Atg5*. c, Degradation levels of α-synuclein protein in SIDT2-overexpressing N2A cells treated with siRNA against

Atg5 or control siRNA (n = 3). d, Immunoblotting of Atg13 in *Atg13* KO N2A cells. e, Immunoblotting of LC3 in WT and *Atg13* KO N2A cells cultured in normal or starvation medium with or without bafilomycin A1, indicating that macroautophagy is abrogated in the *Atg13* KO cells. f–h, Degradation levels of α-synuclein (f), p62 (g), and ΔG LC3, a mutant LC3 the C-terminal glycine of which is deleted (the mutant does not convert to LC3-II). (h) proteins in SIDT2-overexpressing *Atg13* KO N2A cells (n = 3). *$p < 0.05$, **$p < 0.001$.

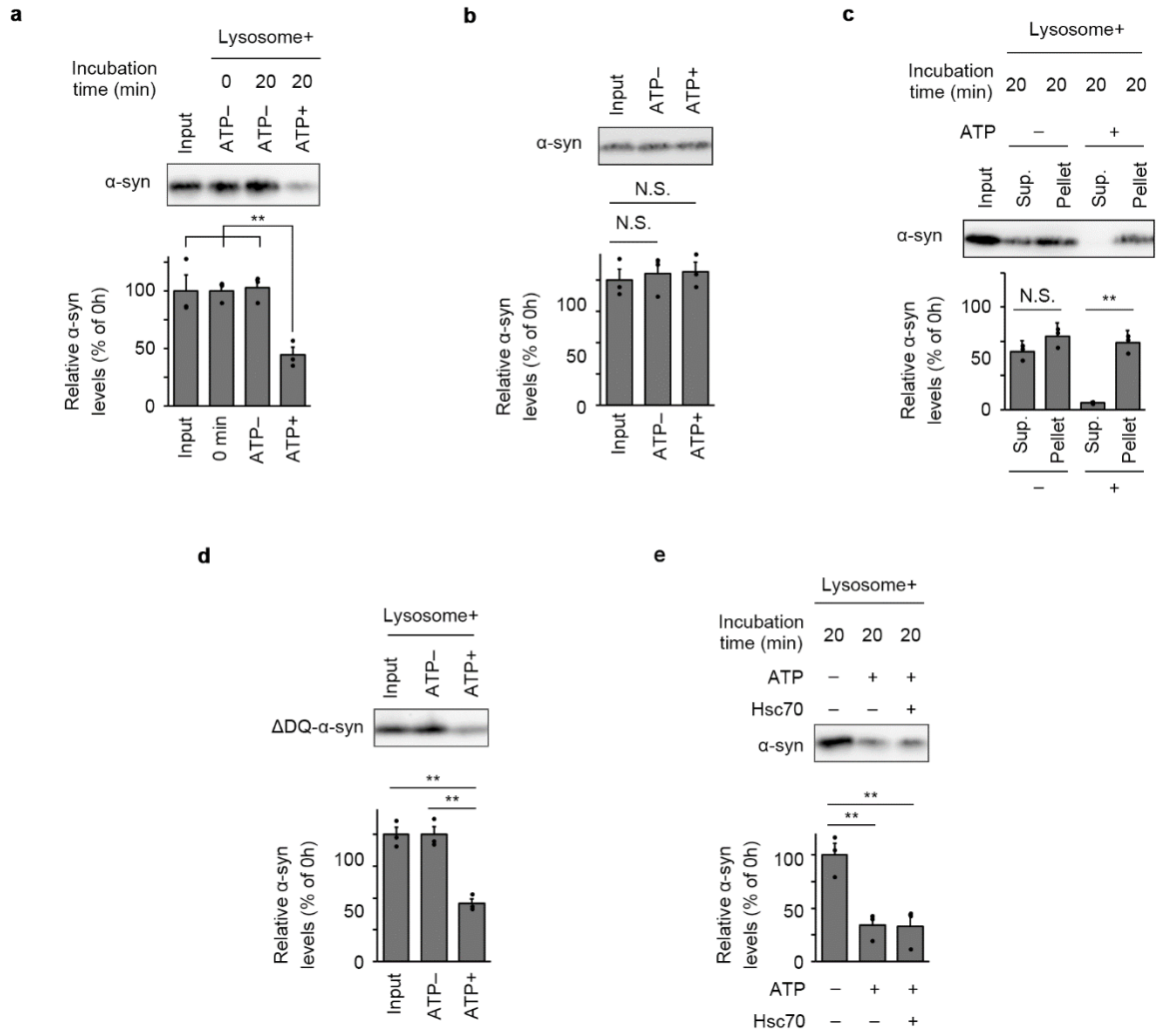

Extended Data Fig. 5 Assays using isolated lysosomes derived from mouse brain tissues.

a, Degradation of α-synuclein protein by isolated lysosomes derived from mouse brain (n = 3). b, Levels of α-synuclein protein incubated in the external solution of isolated lysosomes pretreated in the absence or presence of ATP (n = 3). c, Levels of α-synuclein protein in pellet of isolated lysosomes and external solution following co-incubation with the α-synuclein protein (n = 3). d, Degradation of recombinant mutant α-synuclein protein that lacks the KFERQ-like motif by isolated lysosomes (n = 3). e, Degradation levels of recombinant WT α-synuclein protein by isolated lysosomes with or without Hsc70 chaperone (n = 3). **p < 0.001.

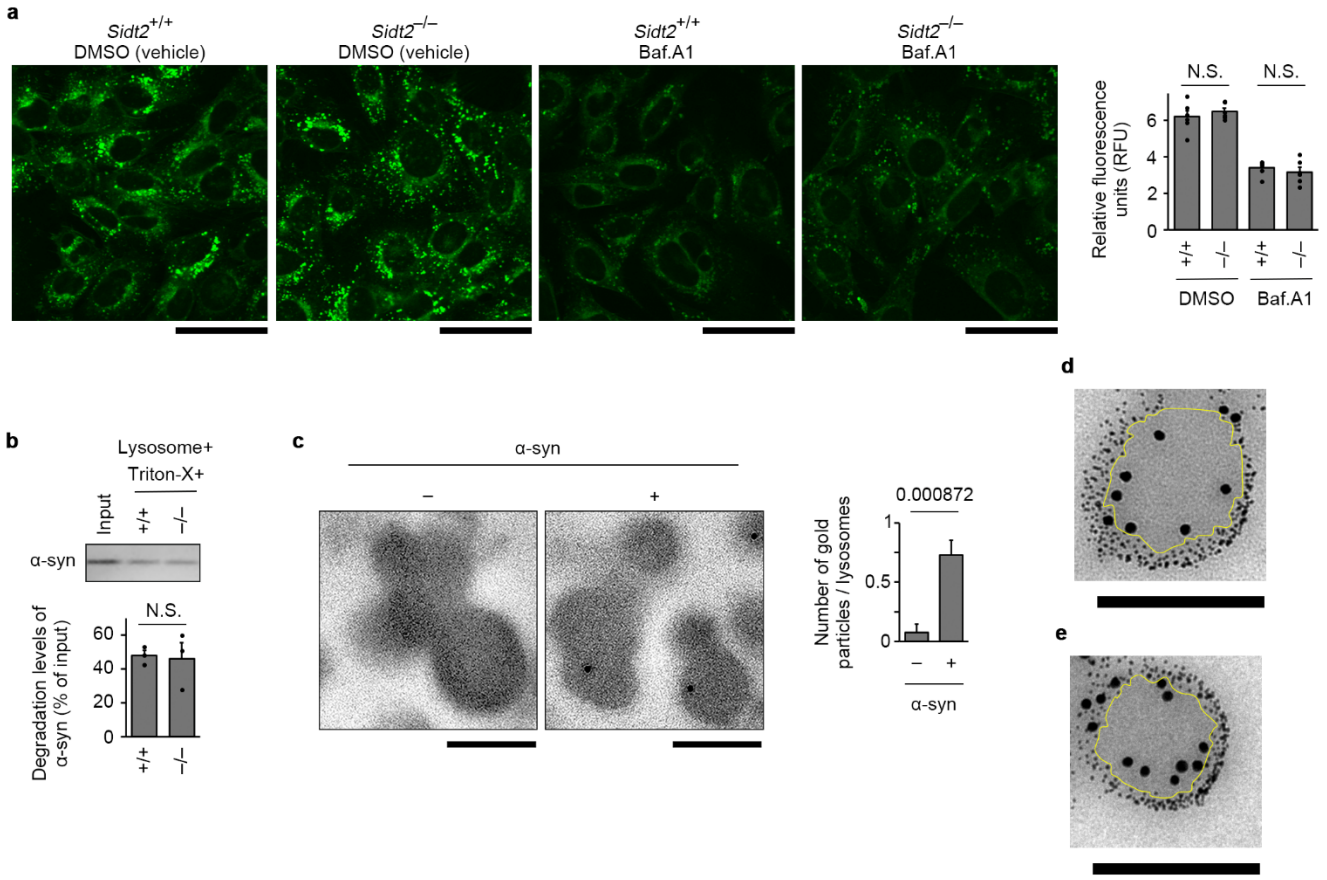

Extended Data Fig. 6 SIDT2 does not affect the intralysosomal proteolytic capacity, and protein degradation by isolated lysosomes takes place inside the lumen of lysosomes.

a, Acidity of lysosomes in *Sidt2*$^{+/+}$ and *Sidt2*$^{-/-}$ MEFs treated with bafilomycin A1 or DMSO (n = 6). Bars represent 50 μm. b, Degradation levels of α-synuclein protein incubated with dissolved isolated lysosomes derived from *Sidt2*$^{+/+}$ or *Sidt2*$^{-/-}$ MEFs (n = 3). c–e, Post-embedded immunoelectron microscopy image of α-synuclein protein in isolated lysosomes co-incubated with (c–e) or without (c) recombinant α-synuclein protein in the presence of ATP. Bars represent 200 nm. Five-nanometre gold particles were co-incubated with lysosomes and α-synuclein protein in the presence of ATP, followed by immunoelectron microscopy against α-synuclein protein using 10 nm gold particles (d, e). Five-nanometre gold particles were stuck on the surface of lysosomes, while 15 nm gold particles indicating α-synuclein protein were seen in the luminal area of the lysosomes. The yellow line indicates the approximate delimitation between the inside and outside of lysosomes.

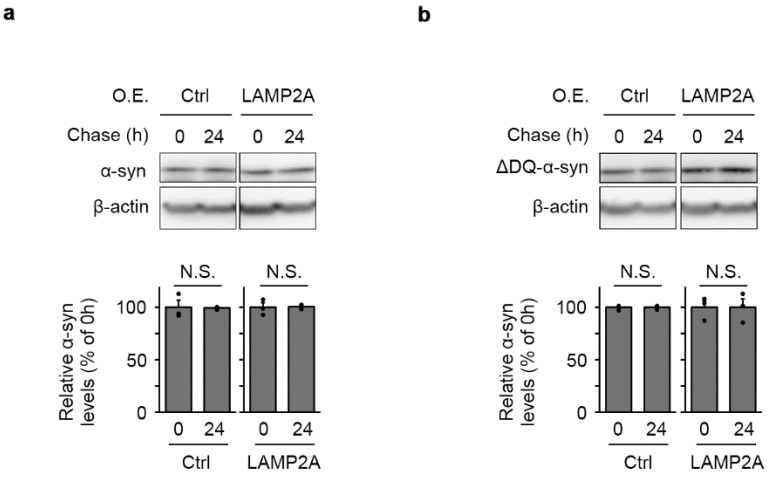

Extended Data Fig. 7 LAMP2A does not accelerate proteolysis in N2A cells.

a, Degradation levels of α-synuclein protein in N2A cells overexpressing LAMP2A, using the Tet-Off system (n = 3). b, Degradation levels of mutant α-synuclein protein that lacks the KFERQ-like motif in N2A cells overexpressing LAMP2A (n = 3).

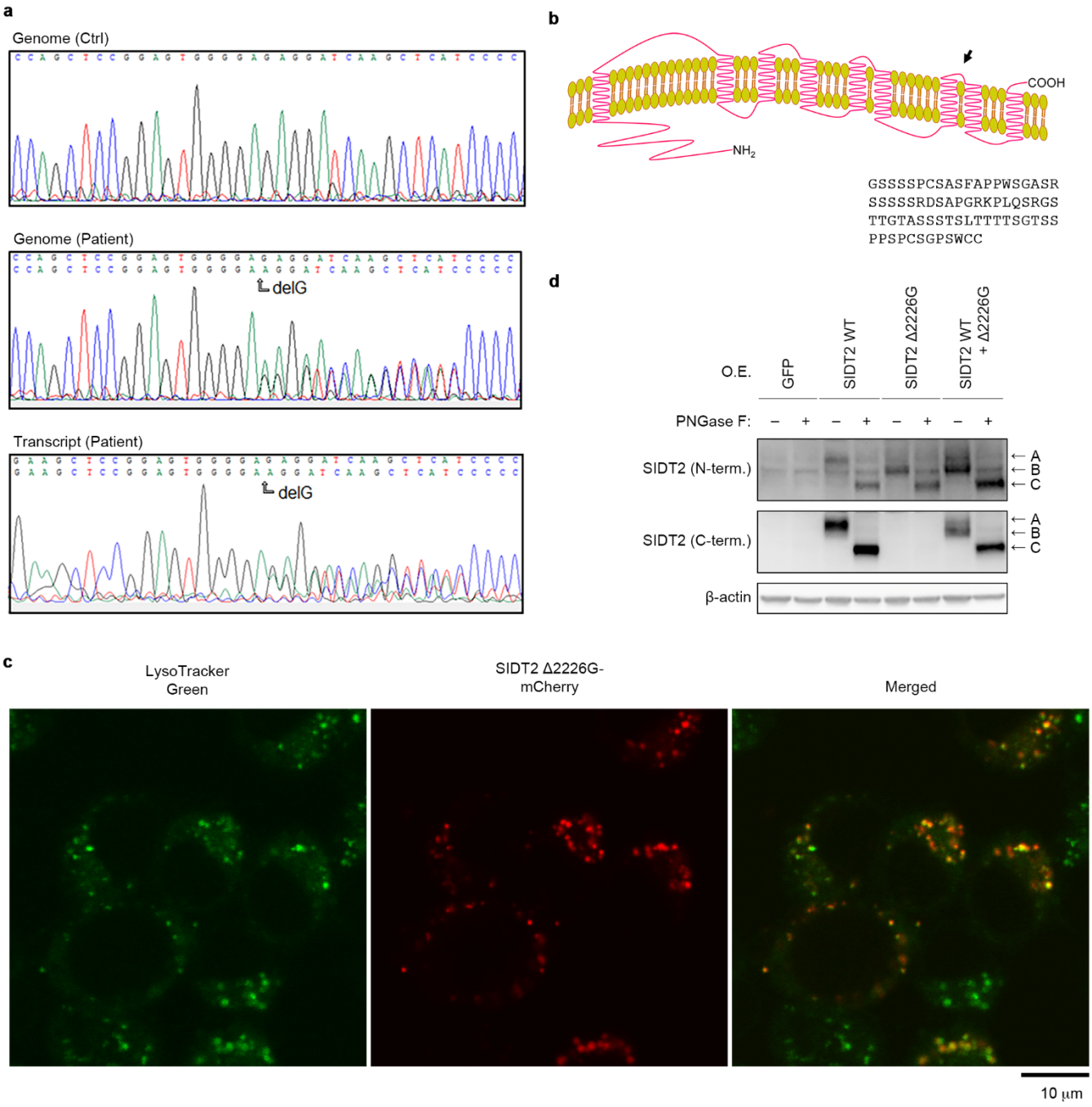

Extended Data Fig. 8 Characterization of rimmed vacuolar myopathy patient harbouring Δ2226G mutation in SIDT2 and the mutant SIDT2.

a, Sanger sequencing chromatogram of a control biopsy and the proband showing the heterozygous Δ2226G frameshift mutation in *SIDT2,* and direct sequencing chromatogram of the patient's *SIDT2* transcript. This variant was not listed in any of the following public databases as of mid-March 2020: dbSNP, 1000 Genomes,

gnomAD, the Human Gene Mutation Database, and ClinVar. b, A schematic of SIDT2 protein and sequence of additional aberrant amino acid residues produced by the Δ2226G mutation in SIDT2. The arrow indicates the site of mutation in the patient. c, Localization of Δ2226G SIDT2–mCherry in N2A cells. d, Glycosylation of WT and Δ2226G SIDT2.

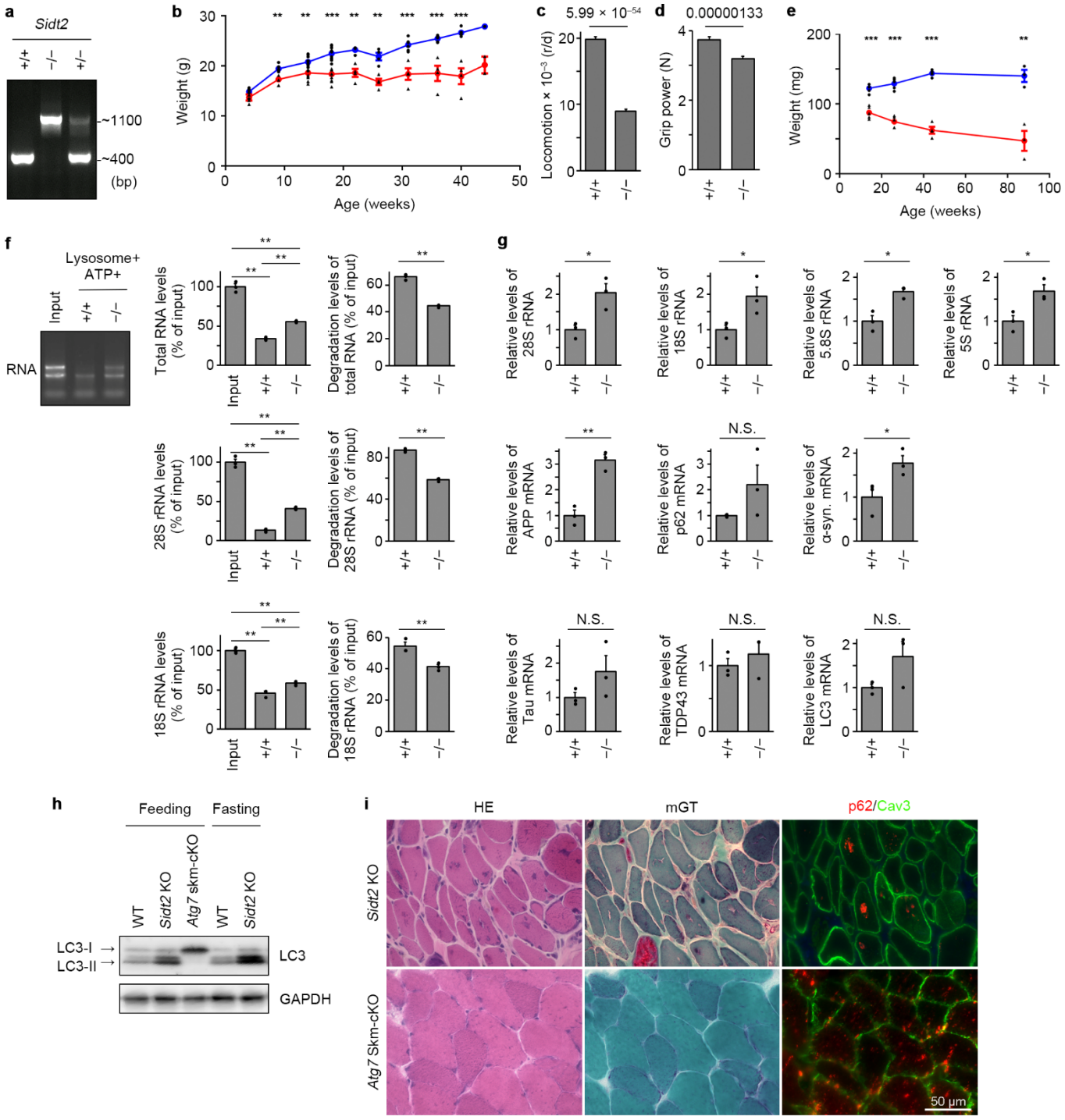

Extended Data Fig. 9 Characterization of *Sidt2* knockout mice.

a, Genotyping of *Sidt2* by PCR. ~400 bp: WT allele-specific band, ~1,100 bp: KO allele-specific band. b, Growth curves of *Sidt2*$^{+/+}$ and *Sidt2*$^{-/-}$ mice (n = 1–11). c, Locomotor activities of *Sidt2*$^{+/+}$ and *Sidt2*$^{-/-}$ mice (+/+ n = 154 from 11 mice, −/− n = 126 from 9 mice). d, Grip strength of *Sidt2*$^{+/+}$ and *Sidt2*$^{-/-}$ mice (+/+ n =

110 from 11 mice, –/– n = 90 from 9 mice). e, Changes in weight of the gastrocnemius of *Sidt2*$^{+/+}$ and *Sidt2*$^{-/-}$ mice (n = 3–5). f, Degradation levels of RNA by isolated lysosomes derived from *Sidt2*$^{+/+}$ or *Sidt2*$^{-/-}$ mouse skeletal muscles (n = 3). g, Levels of RNA in gastrocnemius of *Sidt2*$^{+/+}$ or *Sidt2*$^{-/-}$ mice (n = 3). h, Immunoblotting of LC3 in feeding and fasting *Sidt2*$^{+/+}$ and *Sidt2*$^{-/-}$ mouse skeletal muscles. i, Comparison of skeletal muscle pathology of *Sidt2*$^{-/-}$ mice and *Atg7* skeletal muscle conditional KO mice. Rimmed vacuoles were not observed, and p62 deposits were more diffusely observed in macroautophagy-deficient muscles, compared with the level in *Sidt2*$^{-/-}$muscles. *$p < 0.05$, **$p < 0.001$, ***$p < 0.0001$.

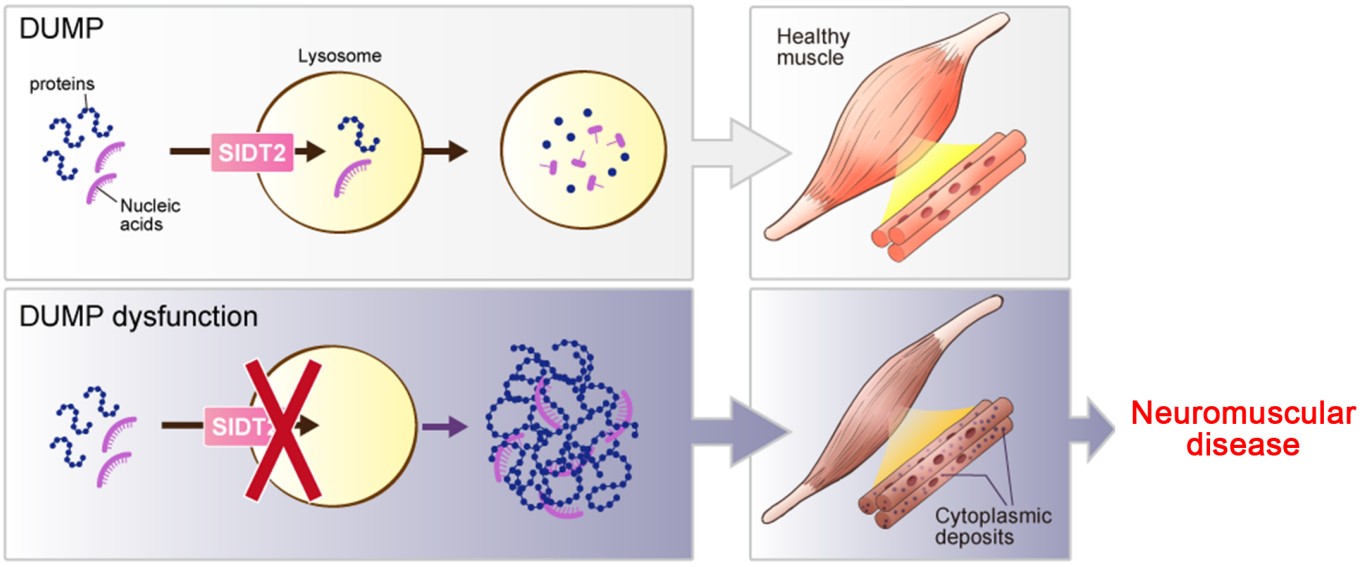

Extended Data Fig. 10 A schematic of DUMP and its dysfunction leading to rimmed vacuolar myopathy. Proteins and nucleic acids are directly taken up into lysosomes via SIDT2, followed by their degradation by luminal hydrolases. This process, DUMP, maintains homeostasis *in vivo* (upper panel). Impairment in DUMP caused by mutation or deficiency in SIDT2 results in accumulation of intracellular deposits in the cytoplasm and induces neuromuscular dysfunction, leading to myopathy and neuropathy with rimmed vacuoles (lower panel).

Methods

siRNAs. siRNAs for *Egfp* (siCtrl) (targeting sequence: 5′- CAGCACGACUUCUUCAAGU-3′), mouse *Sidt2* (siSIDT2: targeting sequence: 5′- GAGUUUCCGUCCAGUAUUU-3′), mouse *Sidt2* (siSIDT2-2: targeting sequence: 5′-GUACCUCUACCAAAAAGUG-3′), mouse *Atg5* (targeting sequence: 5′-GAAAAUGGAUUUCGUUAUA-3′), mouse *Lamp2a* (targeting sequence: 5′-GACTGCAGTGCAGATGAAG-3′), mouse *Vps4a* (targeting sequence: 5′-CAACCCUAGCGUUAUGAUU-3′) and mouse *Vpa4b* (targeting sequence: 5′-CUACCUUGCGAGUGCUACA-3′) were purchased from JBioS.

Plasmids. pCI-neo vectors containing *Egfp*, WT and mutant forms of mouse *Sidt2* and *Lamp2a* were prepared as described previously[6,8,15,16]. pCI-neo vector containing WT human *SIDT2* was prepared by subcloning cDNA encoding human *SIDT2* into pCI-neo mammalian expression vector (Promega, E1841). pCI-neo-human Δ2226G *SIDT2* was generated by mutagenesis using Pfu Turbo DNA Polymerase (Agilent, 600250), in accordance with the manufacturer's instructions. pTRE-Tight vectors containing sequences coding each of FLAG-tagged proteins, pTRE-Tight-*α-synuclein-mCherry*, pTRE-Tight-*α-synuclein-Egfp-mCherry*, pEGFP-N1-*Lamp1* and pmCherry-N1-human Δ2226G *SIDT2*, were generated by subcloning each construct into pTRE-Tight, pEGFP-N1 or pmCherry-N1 vector, respectively. pTRE-Tight-ΔNR *Gapdh* was generated by introducing a mutation into pTRE-Tight-*Gapdh* by mutagenesis. All resulting plasmid constructs were analysed by sequencing.

Cell lines. The *Atg5*$^{-/-}$ mouse embryonic fibroblasts (MEFs) and *Atg5*$^{+/+}$ MEFs were kind gifts from Prof. Noboru Mizushima (The University of Tokyo)[31]. The *Atg13* KO N2A cells were generated using the CRISPR/Cas9 system. The sequence for sgRNA against *Atg13* (5′-GTAGGGAGATTCTATGGAGT-3′) was cloned into pSpCas9(BB)-2A-Puro (PX459) V2.0 plasmid (Addgene, 62988), which was transfected into N2A cells using PEI. The cells were then cloned by limiting dilution and cultured. The resultant KO cells were analysed by immunoblotting and sequencing. *Sidt2*$^{-/-}$ and *Sidt2*$^{+/+}$ MEFs were prepared from mouse embryos of the respective genotype on embryonic days 13.5–14.5, and immortalized by transfection of SV40 large T antigen-expressing vector (pBSSVD2005, Addgene, 21826). All cell lines were grown in Dulbecco's

modified Eagle's medium (DMEM, Gibco, C11995500) supplemented with 10% foetal bovine serum.

Antibodies. The following primary antibodies were used in this study: mouse monoclonal anti-DYKDDDDK tag antibody (1E6, Wako, 012-22384), mouse monoclonal anti-ß-actin antibody (AC-15, Sigma-Aldrich, A1978), rabbit monoclonal anti-Atg5 antibody (EPR1755(2), Abcam, ab108327), rabbit polyclonal anti-Atg13 antibody (Sigma-Aldrich, SAB4200100), rabbit monoclonal anti-LC3B antibody (D11, Cell Signaling Technology, 3868S), goat polyclonal anti-GST antibody (GE Healthcare, 27457701), rabbit polyclonal anti-α-synuclein antibody (Sigma-Aldrich, AB5038P), mouse monoclonal anti-Tau antibody (Tau46, Cell Signaling Technology, 4019S), rabbit monoclonal anti-LIMPII antibody (EPR12080, abcam, ab176317) and rabbit polyclonal anti-SIDT2 antibody raised against the N-terminus of human SIDT2 (Abnova, PAB27211). The production of rabbit polyclonal antibody against an amino acid sequence corresponding to the N-terminus region of mouse SIDT2 (NVSQKDAEFERTYA) was outsourced to Eurofins. Rabbit polyclonal antibody against an amino acid sequence corresponding to the C-terminal region of both human and mouse SIDT2 (DLDTVQRDKIYVF) was produced as previously described[15].

Immunoblotting. Protein samples were separated by SDS-PAGE and transferred on PVDF membranes (Bio-Rad, 1620177; or Wako, 033-23433). PVDF membranes were then blocked with 3% bovine serum albumin in DPBS or 5% skim milk in PBS containing 0.1% Tween 20, followed by incubation with primary antibodies in either of the blocking buffers overnight at 4°C. The membranes were then washed with 0.1% Tween 20 in PBS and probed with horseradish peroxidase-conjugated secondary antibodies (Pierce, 31430 or 31460). Signals were then visualized with ImmunoStar Zeta (Wako, 295-72404) or ImmunoStar LD (Wako, 290-69904), and detected using FluorChem chemiluminescence imaging system (Alpha Innotech) or FUSION chemiluminescence imaging system (Vilber-Lourmat). The signal intensity was quantified using FluorChem software or FUSION software.

Measurement of degradation levels of radiolabelled total proteins in cultured cells. A total of 3.0×10^4

cells/well of *Atg5*$^{+/+}$ MEFs or 2.0 × 10^4 cells/well of Atg5$^{-/-}$ MEFs were seeded in 24-well plates (FALCON, 353047). The following day, 37 kBq/well leucine, L-[4,5-^{3}H(N)]- (PerkinElmer, NET135H) were added to the medium and the cells were radiolabelled for 48 h. After 48 h of labelling, the cells were washed with 500 µl/well of medium containing 8 mM unlabelled leucine (Sigma-Aldrich) and incubated in another 500 µl/well of the same medium for 24 h. Following this incubation, the cells were collected with 500 µl/well of trypsin (Gibco, 25200-056) and mixed with the same volume of 10% trichloroacetic acid (TCA, Wako, 207-04955). The samples were then chilled on ice, centrifuged at 9,100 rpm and 4°C for 10 min, and the TCA-insoluble fraction was collected. The same procedures were also performed soon after the labelling (0 h) and TCA-insoluble radioactivity for all samples was measured using Tri-Carb 3100TR (Packard). The degradation levels of protein were measured as the relative decline in radioactivity between 0 and 24 h. In experiments using siRNA, 10 pmol/well siRNA was transfected into cells 4 h prior to radiolabelling, using Lipofectamine 3000 Reagent (Thermo Fisher Scientific, L3000-015), in accordance with the manufacturer's instructions.

Measurement of proteolysis in cultured cells using Tet-Off system. A total of 1.5 × 10^5 cells/well of N2A cells, HeLa Tet-Off Advanced cells (Clontech, 631156) or *Atg13* KO N2A cells were seeded in 12-well plates (FALCON, 353043). The cells were transfected with plasmids using polyethyleneimine (PEI, Polysciences, 24765-2) the following day, and treated with 1 µg/ml doxycycline (Clontech, 631311) another day later to stop the expression of the FLAG-tagged proteins. The cells were then incubated for 8 h to exclude the effect of mRNA degradation and the samples defined as "0 h" in the experiment were collected. The cells for samples at other time points were further incubated and collected at each of the indicated time points. The plasmids transfected to N2A cells were 0.16 µg/well of pTet-Off vector, 0.02 µg/well of pTRE-Tight vector expressing each FLAG-tagged protein and pCI-neo vector expressing EGFP, WT, 3YS, 3RS or S564A mouse SIDT2. For experiments using inhibitors, 50 µg/ml cycloheximide (Sigma-Aldrich, C1988-1G) or 50 µg/ml pepstatin A (Peptide Institute, 4397-v) and 50 µg/ml E64d (Peptide Institute, 4321-v) were added to the medium at the time point "0 h". For the experiment shown in Figure 3g, N2A cells were transfected with

0.10 µg/well of pTet-Off vector, 0.02 µg/well of pTRE-Tight-*α-synuclein*-FLAG and 0.08 µg/well of pCI-neo vector expressing EGFP or human Δ2226G SIDT2. For the experiment shown in Figure 3k, N2A cells were transfected with 0.10 µg/well of pTet-Off vector, 0.02 µg/well of pTRE-Tight-*α-synuclein*-FLAG, 0.02 µg/well of pCI-neo-WT human *SIDT2* and 0.08 µg/well of pCI-neo vector expressing EGFP or human Δ2226G SIDT2. For experiments using siRNAs, N2A cells were transfected with 0.10 µg/well of pTet-Off vector, 0.05 µg/well of pTRE-Tight-*α-synuclein*-FLAG, 0.05 µg/well of pCI-neo vector expressing EGFP or mouse SIDT2, and 10 pmol/well of siRNA using Lipofectamine 3000 Reagent, in accordance with the manufacturer's instructions. The plasmids transfected to HeLa Tet-Off Advanced cells were 0.10 µg/well of pTRE-Tight-α-synuclein-FLAG and 0.10 µg/well of pCI-neo vector expressing EGFP or mouse SIDT2.

Preparation of recombinant GST and GST-tagged proteins. The GST and GST-tagged proteins were prepared as previously described[16], with slight modifications. Briefly, the proteins were expressed in Rosetta2 (DE3) competent cells (Millipore, 71397) using pGEX-6P-1 vector and the protein expression was induced with 500 µM isopropyl-ß-D(-)-thiogalactopyranoside (IPTG, Wako, 094-05144). The cells were incubated at 25°C for 17 h and harvested by centrifugation. The cells were then suspended in PBS containing 1% Triton-X and protease inhibitors (Roche) and lysed by sonication. The sample was then centrifuged for 10 min at 18,000×g and 4°C, and the proteins were purified from the supernatant using Glutathione Sepharose 4B (GE Healthcare, 17-0756-01). Purified proteins were then incubated on ice for 10 min in 1 M NaCl, and then the buffer was substituted with PBS using Slide-A-Lyzer Dialysis Cassette, 10,000 MWCO, 0.5 mL (Thermo Fisher Scientific).

Pull-down assay. Glutathione Sepharose 4B was blocked with 3% bovine serum albumin in PBS overnight at 4°C and washed three times with PBS containing 1% Triton-X 100. Fifteen micrograms of recombinant His-tagged α-synuclein protein was then incubated with 8 nM GST or GST-tagged proteins and the blocked beads for 18 h at 4°C in PBS containing 1% Triton-X 100. Following this incubation, the beads were washed with the same buffer three times and the pulled-down protein was extracted using SDS sample buffer (10

mM Tris, pH 7.8, 3% SDS, 5% glycerol, 0.02% bromophenol blue and 2% 2-mercaptoethanol).

Fluorescence microscopy. For the experiment shown in Figure 1j, 3.0×10^5 cells/dish of N2A cells were seeded in 35 mm glass-bottomed dishes (IWAKI, 3970-035) and the cells were transfected with 0.16 μg/well of pmCherry-N1-human Δ2226G *SIDT2* with 0.24 μg/well of pCI-neo (empty vector). The following day, the cells were treated with LysoTracker Green DND-26 (Life Technologies, L7526) to label lysosomes and analysed using an FV10 confocal microscope (Olympus). For the experiment shown in Extended Data Figure 4a, 3.0×10^5 cells/dish of N2A cells were seeded in 35 mm glass-bottomed dishes, and the cells were transfected with 0.28 μg/dish of pTet-Off vector, 0.04 μg/dish of pTRE-Tight-*α-synuclein-mCherry*, 0.04 μg/well of pEGFP-N1-*Lamp1* and 0.04 μg/well of pCI-neo-mouse *Sidt2* the following day, and treated with 1 μg/ml doxycycline another day later. The next day, the fluorescence in single cells was chased using DeltaVision Elite (Applied Precision). For the experiment shown in Extended Data Figure 4b, 3.0×10^5 cells/dish of N2A cells were seeded in 35 mm glass-bottomed dishes, and cells were transfected with 0.32 μg/dish of pTet-Off vector, 0.04 μg/dish of pTRE-Tight-*α-synuclein-Egfp-mCherry*, 0.04 μg/well of pCI-neo (empty vector) or pCI-neo-mouse *Sidt2* the following day, and treated with 1 μg/ml doxycycline another day later to stop the expression of α-synuclein-EGFP-mCherry. The next day, the cells were treated with LysoTracker BlueDND-22 (Life Technologies, L7525) to label lysosomes and analysed using an FV10 confocal microscope.

Measurement of autophagic flux. For the experiment shown in Extended Data Figure 3a to measure autophagic flux in a steady-state level, 1.5×10^5 cells/well of WT N2A cells were seeded in 12-well plates. The following day, 0.16 μg/well of pCI-neo (empty vector), 0.02 μg/well of pCI-neo (empty vector) or pCI-neo-mouse *Sidt2*, 0.02 μg/well of pMRX-IP-GFP-RFP-LC3ΔG[32] transfected using PEI, and fluorescence was measured 2 days later using SpectraMax i3x (Molecular Devices). Autophagic flux was measured as the ratio of fluorescence between GFP and RFP in each well. The experiment in Extended Data Figure 3e to analyse whether the cells are capable of driving autophagy[33]. Briefly, 1.5×10^5 cells/well of WT or *Atg13*

KO N2A cells were seeded in 12-well plates, and the medium was changed to amino acid starvation medium (Wako, 048-33575) with or without 100 nM bafilomycin A1, or normal medium as a control, for 2 h. The samples were then subjected to immunoblot against LC3 and autophagic flux was analysed as the difference in the relative levels of LC3-II and LC3-I.

In vitro reconstitution of direct uptake and degradation of protein by isolated lysosomes. Experiments using isolated lysosomes were performed as previously described[6-9,15,16,34] with slight modifications. Briefly, lysosomes were isolated from MEFs, N2A cells, mouse brain or skeletal muscles using Lysosome Enrichment Kit for Tissue and Cultured Cells (Thermo Scientific, 89839) and suspended in 300 mM sucrose. Lysosomes were then mixed with 0.1 μg/assay of recombinant α-synuclein (BIOMOL, SE-256) or tau-441 (Wako, 205-20331) protein and 10 mM 3-(N-morpholino)propanesulphonic acid (MOPS, Dojin, 345-01804) buffer (pH 7) with or without 10 mM adenosine 5′-triphosphate disodium salt n-hydrate (ATP-Na, Wako 017-09673) as the final concentration, in 300 mM sucrose, and incubated at 37°C for 0, 5, 10 or 20 min. For the experiment shown in Figure 1o, the suspended lysosomes were preincubated with or without 50 μg/ml pepstatin A and 50 μg/ml E64d for 30 min on ice, and then subjected to the following experiment. For the experiment shown in Figure 2d and Extended Data Figure 5e, the suspended lysosomes were preincubated with or without 1.0 μg/assay of recombinant His-tagged Hsc70 protein for 30 min on ice, and then subjected to the following experiment. For the experiment shown in Extended Data Figure 5b, isolated lysosomes were incubated at 37°C for 20 min in the presence or absence of ATP and precipitated by centrifugation. The supernatant was collected and then incubated with 0.1 μg/assay of recombinant α-synuclein protein at 37°C for 20 min. For the experiment shown in Extended Data Figure 6b, the isolated lysosomes suspended in 300 mM sucrose were dissolved in citrate buffer containing 1% Triton-X as the final volume, and then incubated with 0.1 μg/assay of recombinant α-synuclein at 37°C for 5 min. For the experiments shown in Figure 4i and Extended Data Figure 9f, lysosomes were isolated from skeletal muscles of the lower extremities of mice and subjected to the following experiments. For the degradation of RNA, 5.0 μg/assay of total RNA was used. In the experiments using lysosomes derived from distinct samples, the amount of

lysosomes was confirmed by immunoblotting on LIMPII.

Measurement of lysosomal pH. A total of 2.0 × 10^5 cells/well of *Sidt2*$^{+/+}$ and *Sidt2*$^{-/-}$ MEFs were seeded in 35 mm glass-bottomed dishes, and cells were treated with or without 100 nM bafilomycin A1, followed by 15 min of treatment with 1 μM LysoSensor Green DND-189 (Thermo Fisher Scientific, L7535) 1 h later. The medium was then washed out, cells were incubated for 1 h and lysosomal pH was analysed as relative fluorescence units using an FV10 confocal microscope and ImageJ software.

Immunoelectron microscopy. Immunoelectron microscopy was performed as previously described[6-9]. Briefly, isolated lysosomes were incubated in the presence of ATP with or without recombinant α-synuclein protein and 5 nm gold particles (Cytodiagnostics, G-5-20), and precipitated by centrifugation. Lysosomes were then fixed with 0.1% glutaraldehyde and 4% paraformaldehyde in 0.1 M phosphate buffer overnight at 4°C, dehydrated in a series of water/ethanol mixtures to 100% ethanol and embedded in LR White (Nisshin EM, 3962). The samples were then sectioned at a thickness of 100 nm and collected on 400-mesh nickel grids. The sections were subsequently immunolabelled with anti-α-synuclein antibody (Cell Signaling Technology, 2628 for Fig. 1p and Extended Data Fig. 6d; and Abcam, ab138501 for Extended Data Fig. 6c and e), followed by 15 nm gold-labelled goat anti-rabbit IgG (H+L) (Amersham), and observed using a Tecnai Spirit transmission electron microscope (FEI) at 80 kV.

Preparation of recombinant ΔDQ mutant α-synuclein protein. The ΔDQ α-synuclein recombinant protein was prepared as previously described[6], with slight modifications. Briefly, Rosetta2 (DE3) competent cells (Millipore, 71397) were transformed with pGEX-6P-1-ΔDQ α-synuclein and the protein expression was induced with 500 μM isopropyl-β-D(-)-thiogalactopyranoside (IPTG, Wako, 094-05144). The cells were incubated at 25°C overnight and harvested by centrifugation. The cells were then suspended in PBS containing 1% Triton-X and protease inhibitors and lysed by sonication. The sample was then centrifuged for 10 min at 18,000×g and 4°C, and GST-tagged ΔDQ α-synuclein protein was purified from the

supernatant using Glutathione Sepharose 4B (GE Healthcare, 17-0756-01). ΔDQ α-synuclein protein was then cleaved from GST using PreScission Protease (GE Healthcare, 27-0843-01).

Patient. All clinical information and materials used in this study were obtained for diagnostic purposes with written informed consent. The ethics committee of the National Center of Neurology and Psychiatry (NCNP) approved this study and the use of human subjects for this study. All relevant ethical regulations were followed. We reviewed the medical information obtained from interviews conducted by physicians and evaluated the patient's clinical manifestations, disease course and laboratory data.

Skeletal muscle imaging. Skeletal muscle MRI data in digital imaging and communications in medicine format were available as part of the clinical information at the time of muscle pathology diagnosis at the NCNP.

Mutation analysis. At the NCNP, whole-exome sequencing (WES) analysis has been performed in 2,131 undiagnosed cases of suspected hereditary muscle disease using genomic DNA from blood or biopsied muscle samples (Neurology 2020, in press). We screened this WES database for the variants in SIDT2 and evaluated them according to the following variables: (1) mutation effect (i.e., splicing, start lost, stop gained or lost, frameshift, nonsynonymous codon change, and codon insertion or deletion); and (2) variation frequency, < 0.001 in a public database [Genome Aggregation Database (gnomAD), 1000 Genomes Project, or Exome Sequencing Project v. 6500 (ESP6500)] and <0.01 for in-house data[35]. The identified variants were confirmed by Sanger sequencing. Expression of the transcript with variants was analysed by direct sequencing and cloning of the RT-PCR products of the SIDT2 transcript from skeletal muscles of patients. Primer sequences for the PCR are available upon request.

Muscle pathology. Muscle samples were taken from the deltoid muscle of the patient and the quadriceps femoris, gastrocnemius and tibialis anterior muscles from mice and then frozen in isopentane cooled in

liquid nitrogen[36]. Histological analysis was performed as previously described[37]. Electron microscopic observation of the hamstring muscles from the mice was performed in line with a previously reported protocol[38]. Immunofluorescence of skeletal muscles was performed in accordance with previously reported methods[27]. For the morphometric analysis, we stained frozen transverse sections of gastrocnemius muscles for caveolin 3, LC3 and p62 and took photographs under a Keyence BZ X-700 microscope. Five randomly selected images with caveolin 3 staining per mouse were used to measure fibre diameters using ImageJ software (NIH). The minimal inner diameters of 2,000 myofibres from each mouse were measured. Images of whole muscles were used to measure RVs and inclusion by LC3 and p62 staining, respectively[39]. The primary antibodies used in this study were as follows: Anti-LAMP2 mouse-Mono (H4B4, Santa Cruz), Anti-p62 Rb-poly (BML-PW9860, Enzo), Anti-LC3 Rb-poly (NB100-2220, Novus), Anti-Cav3 goat-poly (N-18 Santacruz), Anti-amyloid mouse-Mono (6E-10, Covance) and Anti-TDP-43 Rb-poly (Protein Tech).

In vitro deglycosylation of SIDT2 using PNGase F. N2A cells expressing GFP, WT human SIDT2, Δ2226G human SIDT2, or WT and Δ2226G human SIDT2 were lysed with 1% Triton X-100 lysis buffer (50 mM Tris-HCl, pH 7.5, 150 mM NaCl, 5 mM EDTA, 1% Triton X-100) containing protease inhibitors (Complete, EDTA free; Roche Applied Science, 1873580), and treated with PNGase F (New England BioLabs, P0704S) at 37°C for 4 h or left untreated. Following the treatment, the samples were subjected to immunoblotting.

Generation of *Sidt2* knockout mice. The *Sidt2*$^{-/-}$ mice were generated using the CRISPR/Cas9 system. The sequences for sgRNA against two distinct sites in exon 13 (5′-ACTGGACTCCATGAGCTCCG-3′) and exon 26 (5′-CGACTTGGACACAGTACAGC-3′) of SIDT2 were designed using the CRISPR DESIGN program (http://crispr.mit.edu) and cloned into the pX330 plasmid (Addgene, 42230). The plasmids were then directly injected into pronuclei of B6C3F1 fertilized eggs. The genotype of the resultant KO mice (deletion between exon 13 and 26) was confirmed by PCR using following primers; 5′-GGGACCTCTCCTACAGTTACCAGG-3′, 5′-CCGCAGAGGCAACTCCAAGGCTC-3′, and 5′-CGCAGAGTCCAGGGAGCACAAC-3′. The KO mouse was backcrossed with C57BL/6J mice for at least

eight generations before being used in the experiments, except for the data shown in Fig. 4d–h, Extended Data Fig. 9f g, and i (three generations). We confirmed that rimmed vacuoles were also observed in the backcrossed mice (eight generations). All animal experiments were approved by the animal committee of the NCNP and all relevant ethical regulations were followed. Mice were maintained under specific pathogen-free conditions.

Physiological examination of mice. Grip strength of combined forelimbs/hindlimbs and voluntary locomotion within an individual cage using a running wheel were measured as described previously[37]. The contractile properties of the tibialis anterior and gastrocnemius muscles were measured in accordance with previously reported protocols[40,41].

Quantification of relative levels of RNAs in *Sidt2*$^{+/+}$ and *Sidt2*$^{-/-}$ mouse muscles. RNA was purified from frozen sections of mouse gastrocnemius using TRI Reagent (Sigma-Aldrich, T9424), in accordance with the manufacturer's instructions. cDNA was then synthesized using PrimeScript RT Reagent Kit with gDNA Eraser (Perfect Real Time) (TaKaRa, RR047), followed by quantitative PCR using TB Green *Premix Ex Taq* II (Tli RNaseH Plus) (TaKaRa, RR820) and CFX96 Touch Real-Time PCR Detection System (Bio-Rad). The levels of each RNA were normalized by *Gapdh* mRNA levels. The following primers were used for the detection of respective RNAs: 28S rRNA Forward: 5′-TGGGAATGCAGCCCAAAGC-3′, Reverse: 5′-CCTTACGGTACTTGTTGACTATVG-3′, 18S rRNA Forward: 5′-GTAACCCGTTGAACCCCATT-3′, Reverse: 5′-CCATCCAATCGGTAGTAGCG-3′, *App* Forward: 5′-GGAAGCAGCCAATGAGAGAC-3′, Reverse: 5′-GGTTCATGCGCTCGTAGATCA-3′, *p62* Forward: 5′-TGTGGAACATGGAGGGAAGAG-3′, Reverse: 5′-GTGCCTGTGCTGGAACTTTC-3′, α-synuclein Forward: 5′-ATGGATGTGTTCATGAAAGGAC-3′, Reverse: 5′-AACCACTCCTTCCTTAGTTTTG-3′, *Tau* Forward: 5′- CCTGAGCAAAGTGACCTCCAAG-3′, Reverse: 5′-CAAGGAGCCAATCTTCGACTGG-3′, *Tdp43* Forward: 5′-CTCAGTGTATGAGAGGAGTCCGAC-3′, Reverse: 5′-ACACTATGAGGTCAGATGTTTTCTGG-3′, and *Lc3* Forward: 5′-GACGGCTTCCTGTACATGGTTT-3′, Reverse: 5′-TGGAGTCTTACACAGCCATTGC-3′. Specific primers for

5S rRNA, 5.8S rRNA and *Gapdh* were prepared as previously described[8].

***Atg7* skeletal muscle conditional knockout mice.** *Atg7*-flox mice were developed by Prof Komatsu Masaaki (Juntendo University)[42] and MuCre-A mice were developed by Prof Kyoko Koishi (University of Otago)[43] (20877696). Both mice were provided from Riken BioResource Research Center (RBRC02759 and RBRC01386). Mice with skeletal muscle-specific *Atg7* KO were generated by mating.

Preparation of feeding and fasting mice. For starvation, mice were placed in clean cages without food for 30 h (from 9 AM to 3 PM the next day). Water was given ad libitum. Starvation for 30 h resulted in a 10% loss of weight, but no mortality due to starvation occurred.

Statistical analysis. Quantitative data were analysed by Student's t-test for comparison between two groups and by Dunnett's or Tukey's multiple comparison test for more than two groups. All statistical tests are two-sided. All measurements were taken from distinct samples. For immunoblotting and for microscopic images with quantitative data, representative images are shown. Graphs show means, data points and SE.

Data availability

All data generated and used in this study are either included in this article or are available from the corresponding authors upon reasonable request.

Acknowledgements We thank N. Mizushima for constructive advice and suggestions that improved our work, and for providing *Atg5*$^{-/-}$ and *Atg5*$^{+/+}$ MEFs, M. Komatsu for providing *Atg7*-flox mice, K Koishi for providing MuCre-A mice, and M. Shikama and Y Hara for technical assistance. We also thank Edanz Group (https://en-author-services.edanzgroup.com/ac) for editing the English text of a draft of this manuscript. This work was supported by a grant from Japan Agency for Medical Research and Development (AMED)

(JP20dm0107127 to T.K.), Grants-in-Aid for Scientific Research from the Japan Society for the Promotion of Science (16H05146, 16H01211 and 19H05710 to T.K. and 17K07124 to K.W.), Grants-in-Aid for JSPS Research Fellows (17J10610 to Y.F. and 15J06173 to V.R.C.), a Grant-in-Aid for JSPS International Research Fellows (18F18384 to V.R.C.), research grants from Takeda Science Foundation (to Y.F. and T.K.), Intramural Research Grants for Neurological and Psychiatric Disorders (30-5 and 30-9 to T.K., 30-9 and 2-6 to S.N., 2-5 to I.N., and 27-9 to K.W.) from the National Center of Neurology and Psychiatry (Japan), and AMED under Grant Number JP20ek0109490h0001 to I.N. and S.N.

Author contributions Conceptualization: Y.F., S.N., T.K.; Data curation: Y.F., S.N., T.K.; Formal analysis: Y.F., V.R.C., C.K., M.O., S.N., T.K.; Funding acquisition: Y.F., V.R.C., I.N., K.W., S.N., T.K.; Investigation: Y.F., V.R.C., C.K., M.O., H.F., H.K., R.S., K.H., M.T., M.S., I.K.-H., M.I., Y.O., Y.I.-U., T.I.; Methodology: Y.F., V.R.C., R.S., K.H., I.K.-H., K.W., S.N., T.K.; Project administration: Y.F., S.N., T.K.; Supervision: I.N., S.N., T.K.; Validation: Y.F., V.R.C., C.K., S.N., T.K.; Visualization: Y.F., M.O., S.N., T.K.; Writing - original draft: Y.F. and S.N.; and Writing - review and editing: Y.F., S.N., T.K.

Competing interests The authors declare no competing interests.

Additional information

Correspondence and requests for materials should be addressed to T.K. or S.N.

Supplementary information

Supplementary text 1:

Among the various proteins examined, the contribution of SIDT2 to the degradation of tau and α-synuclein protein was clearly indicated, as the protein was markedly degraded under SIDT2 overexpression, while no significant degradation of these proteins was observed in control cells (Fig. 1c, d).

Supplementary text 2:

Because the overexpression of LAMP2A did not affect the degradation rate of α-synuclein, it is likely that CMA was not active under our experimental conditions (Extended Data Fig. 7a, b).

Supplementary text 3:

Basically, all known receptors for both microautophagy and macroautophagy, as well as membrane-bond LC3 in macroautophagy, are degraded along with their substrate as a consequence for their interaction. However, considering that the binding capacity of SIDT2 to the substrate is required for this pathway (Fig. 1h, i) and that the decline in the level of SIDT2 itself is not observed during the process (Fig. 2g), SIDT2 is unlikely to function in a mechanism akin to these known pathways, as well as microautophagy via an as-yet-unknown mechanism. These facts suggest that SIDT2 functions as a transporter, rather than a mere receptor, in this pathway.

Supplementary text 4:

The patient's symptoms began in the third decade of life with gradual progression of muscle weakness and atrophy in the upper and lower extremities. He developed an inability to run at 54 years, and bilateral foot drop and an inability to perform fine handiworks at 59 years of age. His father and son were also affected (Fig. 3a). On electromyography and nerve conduction study, early recruitment and markedly lower amplitudes in motor unit action potential and compound muscle action potential were observed.

Supplementary text 5:

Upon radiography of the patient, hamstring, triceps surae and tibialis anterior muscles were preferentially replaced by fat (Fig. 3b). His vastus lateralis muscles showed marked variation in myofibre size, small group atrophy with several small angulated fibres and pyknotic nuclear clumps, fibrosis and adipose tissue infiltration in endomysium (Fig. 3c). Rimmed vacuoles, in which aggregate-prone proteins were characteristically accumulated with autophagic and lysosomal proteins, were observed in some atrophic

myofibres (Fig. 3d, e). In addition to those myogenic observations, a remarkable deficit of axons of intramuscular nerves was also observed (Fig. 3f).

Supplementary text 6:

The *Sidt2*$^{-/-}$ mice showed smaller size, reduction in locomotor activity and decreased grip strength (Extended Data Fig. 9b–d). A progressive and severe decrease in muscle contraction and gradual reduction in the size of skeletal muscles, indicating the myopathic phenotypes, were also observed (Fig. 4a–d, Extended Data Fig. 9e). Histological analysis revealed that the myofibres were atrophic and varied in size, while no necrotic and regenerating fibres were observed (Fig. 4e). In addition, fibrosis and adipocyte infiltration were also observed (Fig. 4e), all of which were strikingly analogous to those seen in the muscle of the patient. Indeed, rimmed vacuoles immunoreactive to various aggregate-prone proteins and LC3 were observed in the skeletal myofibres of *Sidt2*$^{-/-}$ mice (Fig. 4f). Biochemically, accumulation of α-synuclein was also observed in the skeletal muscle of these mice (Fig. 4g) Ultrastructurally, amorphous inclusions surrounded by multilamellar bodies[27] at the centre of myofibres in *Sidt2*$^{-/-}$ mice were observed (Fig. 4h). Taken together, these features clearly show that SIDT2-deficient mice recapitulate typical symptoms of rimmed vacuolar myopathy.

Supplementary text 7:

In general, all RVMs are thought to be primarily caused through the cytoplasmic accumulation of proteins and other substances that should constitutively be degraded, and aberrancy in the normal functions of lysosomes such as luminal pH and hydrolase activity is not the primary cause of this group of myopathies[25]. This is consistent with the fact that all causative genes of RVMs reported previously encode extralysosomal proteins. To our knowledge, this is the first causative gene of RVM that encodes a lysosomal protein. This is in contrast to the fact that all known causative genes for autophagic vacuolar myopathies other than RVMs encode lysosomal proteins, and those diseases are thought to be caused primarily by aberrancy in the normal functions of lysosomes[25]. Importantly, none of such primary lysosomal myopathies harbours

rimmed vacuoles. These findings strongly suggest that deficiency of SIDT2 causes RVM through impairment in the translocation of degradation substrates from the cytoplasm to the lysosomal lumen by DUMP, rather than through mere impairment in the normal function of lysosomes in the lumen.

Supplementary text 8:

Similar to the observations in the patient, the accumulation of LC3, multilamellar bodies and clusters of autophagosomes were also seen in the cytosolic inclusions of the muscles (Fig. 4f, h). These features are probably consequences of the secondary induction of macroautophagy in response to inclusion formation, as commonly seen in other rimmed vacuolar myopathies[25,44]. In fact, we observed that macroautophagy was normally activated upon fasting in *Sidt2*$^{-/-}$ mouse muscle (Extended Data Fig. 9h). In addition, histological and immunohistological features of muscle in skeletal muscle-specific conditional *Atg7* KO mice were distinct from those seen in *Sidt2*$^{-/-}$ mice (Extended Data Fig. 9i), further supporting that the myopathic features of *Sidt2*$^{-/-}$ mice and the patient are unlikely to be a consequence of macroautophagy deficiency.